Check for updates

LIMNOLOGY and OCEANOGRAPHY

ASLO

Limnol. Oceanogr. 71, 2026, e70281
© 2026 The Author(s). *Limnology and Oceanography* published by Wiley Periodicals LLC on behalf of Association for the Sciences of Limnology and Oceanography.
doi: 10.1002/lno.70281

RESEARCH ARTICLE

Isotopic constraints on active nitrification in a eutrophic artificially oxygenated lake: Implications for nitrate regeneration and nitrous oxide production

Alessandra Mazzoli,* **Claudia Frey**, **Cameron M. Callbeck**, **Jakob Zopfi**, **Teresa Einzmann**, **Chiara Piantoni**,[a] **Tim J. Paulus**, **Moritz F. Lehmann**

Department of Environmental Sciences, University of Basel, Basel, Switzerland

Abstract

Nitrification is a key process in the aquatic nitrogen (N) cycle, but its products, nitrate (NO_3^-) and nitrous oxide (N_2O), contribute to eutrophication and greenhouse gas emissions, particularly in eutrophic lakes. Variations in in-lake N cycling and N_2O production pathways, as a function of seasonality and artificial oxygenation, remain poorly understood. We investigated nitrification in the artificially oxygenated eutrophic Lake Baldegg, by analyzing NO_3^- and N_2O concentrations and isotope ratios, and measuring ammonium oxidation rates via ^{15}N tracer incubations over one year. An N isotope mass-balance model revealed that nitrification sustained only 5.3 ± 0.7% of total NO_3^- consumption in the epilimnion, where external N loadings were influential, and considerably more in the hypolimnion (81.6 ± 18.5%) during stratification. Dual NO_3^- isotope signatures ($\Delta\delta^{18}O : \Delta\delta^{15}N \sim 1.5–1.73$) and associated negative NO_3^- isotope anomalies confirmed epilimnetic nitrification, though external inputs partly obscured this signal. During stratification, relatively high hypolimnetic nitrification rates correlated with organic matter export, and seemed linked to sediment resuspension and artificial oxygenation. While sedimentary denitrification/DNRA dominated hypolimnetic NO_3^- reduction (with negligible effects on $\delta^{15}N\text{-}NO_3^-$ and $\delta^{18}O\text{-}NO_3^-$), transient suboxic conditions enabled water column denitrification during stratification (24.1–30.2% of the total hypolimnetic denitrification). High N_2O isotope site-preference values (30–35‰) confirmed hypolimnetic ammonium oxidation as the main N_2O production pathway. During winter overturn, N_2O transport from the hypolimnion caused epilimnetic N_2O oversaturation and atmospheric emissions up to 3.52 μmol m^{-2} d^{-1}. Comparison with other lakes suggests that artificial oxygenation enhances N turnover, manifesting in greater ambient N_2O backgrounds and fluxes to the atmosphere.

Nitrogen (N) contamination has received growing attention due to its deleterious environmental impacts (Gruber and Galloway 2008; Finlay et al. 2013; Stein and Klotz 2016). In aquatic systems, excess reactive N, including nitrate (NO_3^-), nitrite (NO_2^-) and ammonium (NH_4^+), has led to eutrophication, anoxia (Harrison et al. 2009; Li et al. 2014; Xu et al. 2016; Higgins et al. 2018), and increased emissions of nitrous oxide (N_2O), a potent greenhouse gas (Wenk et al. 2016; Zhou et al. 2019; Liang et al. 2022). Anthropogenic activities, especially fertilizer use, now dominate reactive N inputs to coastal and lacustrine systems through leaching and runoff (Harrison et al. 2009). Lakes are particularly important in intercepting and processing N, removing 13.0 Tg N yr^{-1} globally through denitrification and N burial (Harrison et al. 2009); yet, they emit 64.6 ± 12.1 Gg N yr^{-1} as N_2O (Li et al. 2024).

The freshwater N cycle is highly dynamic, encompassing numerous redox reactions and both external and internal processes (McCarthy et al. 2016). Reactive (or fixed) N stimulates algal growth and biomass production, which in turn fuels further N cycling (Stein and Klotz 2016). Organic matter

*Correspondence: alessandra.mazzoli@unibas.ch

[a]Present address: Umwelt und Energie, Kanton Luzern, Lucerne, Switzerland

This is an open access article under the terms of the Creative Commons Attribution License, which permits use, distribution and reproduction in any medium, provided the original work is properly cited.

Associate editor: Werner Eckert

(OM) degradation releases NH_4^+, which is aerobically oxidized to NO_3^- and N_2O via nitrification (Stein and Klotz 2016; Ji et al. 2018). Under suboxic and anoxic conditions, fixed N is removed via denitrification and anammox, or retained within the system by dissimilatory NO_3^- reduction to NH_4^+ (DNRA) (Seitzinger et al. 2006; McCarthy et al. 2016). Environmental and biogeochemical factors within a lake, such as OM export and oxygen (O_2) availability, modulate the occurrence of these processes (Seitzinger et al. 2006; Han et al. 2014), determining the balance between internal N recycling and removal.

Nitrification, the stepwise NH_4^+ oxidation to NO_3^- via hydroxylamine and NO_2^-, is a key component of the lacustrine N cycle, occurring in both the water column and surface sediments (Frame and Casciotti 2010; Small et al. 2013). Nitrification connects N sources (i.e., fixation, external loadings, freshly mineralized NH_4^+) and sinks (e.g., N burial, denitrification, anammox), and produces N_2O and NO_3^- under oxic conditions (Cavaliere and Baulch 2019; Müller et al. 2021). Lacustrine N_2O emissions are generally ascribed to oxidative N_2O production (i.e., associated with nitrification under oxic conditions) near the surface (Huttunen et al. 2001; Liu et al. 2018; Liang et al. 2022). Yet, under low-O_2 conditions (Liang et al. 2022; Li et al. 2022), incomplete denitrification or nitrifier-denitrification can also produce N_2O (Huttunen et al. 2001; Wenk et al. 2016; Li et al. 2024), with the largest yield often near the oxic–anoxic interface (Mengis et al. 1997; Ji et al. 2018). Meanwhile, newly nitrified NO_3^- can be (re)assimilated or denitrified, modulating both the lake's productivity and N removal efficiency (i.e., via coupled nitrification–denitrification) (Botrel et al. 2017; Cavaliere and Baulch 2019). Therefore, enhanced N recycling via nitrification can affect both N_2O production and N loss, actively altering the N budget of a lake. Nonetheless, the controls of fluctuating (or artificially maintained) redox conditions on NO_3^- regeneration, and oxic vs. anoxic N_2O production remain poorly understood.

In this context, O_2 is a crucial modulator of lacustrine nitrification/NO_3^- regeneration, driving seasonal and stratification-dependent shifts in the oxic-anoxic interface location. Sediments typically serve as year-round fixed-N filters via denitrification, whereas the water column assumes this ecosystem function only under suboxic conditions, as seen in eutrophic lakes (Seitzinger et al. 2006). Artificial aeration and oxygenation systems are commonly employed to improve water quality by introducing compressed air or pure oxygen into the hypolimnion, thereby preventing phosphorus (P) release from sediments (Singleton and Little 2006). In Lake Hallwil (Switzerland), for example, winter aeration promotes vertical mixing, whereas hypolimnetic oxygenation maintains thermal stratification and oxic conditions during summer (Mostefa and Ahmed 2012). These conditions support aerobic OM mineralization (i.e., aerobic ammonification) and nitrification, while confining denitrification primarily to the sediments (Han et al. 2014). Artificial aeration enhances benthic nitrification–denitrification in reservoirs and wetlands (Cottingham et al. 1999; Han et al. 2014; Li et al. 2014), yet its effect in natural lakes remains less explored (Huttunen et al. 2001; Liboriussen et al. 2009). To our knowledge, the impact of hypolimnetic oxygenation on nitrification-driven N regeneration and N_2O production in seasonally stratified, artificially aerated, eutrophic lakes remains largely unexamined. One study reported higher N_2O concentrations in oxygenated compared to non-oxygenated hypolimnia (Huttunen et al. 2001), but detailed assessments of seasonal N_2O dynamics are still lacking.

Lake Baldegg, a eutrophic lake in central Switzerland, offers an ideal site for studying nitrification under high N-loading conditions. We investigated the effects of oxygenation on nitrification and associated N_2O production in the water column of Lake Baldegg across seasons. Given the substantial external N loading (197 t N yr^{-1}) (Müller et al. 2021), we hypothesize that aeration/oxygenation intensifies hypolimnetic nitrification and NO_3^- recycling, thereby influencing N removal and N_2O production.

Using ^{15}N tracer experiments, we quantified nitrification rates to capture the NO_3^- production that would otherwise go untraced due to rapid consumption. We combined these direct rate measurements with more integrative dual N and O NO_3^- isotope analyses ($\delta^{15}N$ and $\delta^{18}O$) (Sigman et al. 2005; Casciotti et al. 2008), and an N isotope mass-balance model to quantify the role of nitrification in supporting assimilative and dissimilative NO_3^- consumption (Small et al. 2013). Dual NO_3^- isotope measurements help to discern between NO_3^--consuming processes (e.g., denitrification and assimilation), which produce coupled $\delta^{15}N$-NO_3^- and $\delta^{18}O$-NO_3^- signals, and NO_3^--producing mechanisms (e.g., NO_3^- regeneration by nitrification). The latter yield de-coupled signals, as the sources of N (NH_4^+ from OM mineralization) and O (H_2O and dissolved O_2) are independent and distinct (Lehmann et al. 2004c; Sigman et al. 2005; Wankel et al. 2007). Similarly, natural abundance N_2O isotope measurements (including N_2O site preference; $SP = \delta^{15}N^{\alpha}$-$\delta^{15}N^{\beta}$, where α and β refer to the central and end position, respectively, within the N_2O molecule [McIlvin and Casciotti 2010]) were employed to identify the dominant N_2O production pathway (nitrification vs. incomplete denitrification), and potential N_2O reduction to N_2 (Wenk et al. 2016). Our findings suggest that expanding the nitrification layer into a fully oxygenated hypolimnion drives substantial N_2O accumulation during summer and autumn, highlighting the influence of artificial oxygenation on the N dynamics of Lake Baldegg.

Material and methods

Study site

Lake Baldegg is a small lake (5.22 km^2, max. depth 66 m; Supporting Information Table S1) on the Swiss Plateau with a long history of eutrophication, caused by intensive farming and agricultural practices in its catchment. Nutrient loadings peaked in the 1970s and 1980s, with N and P concentrations

19395590, 2026, 1, Downloaded from https://aslopubs.onlinelibrary.wiley.com/doi/10.1002/lno.70281 by Moritz F. Lehmann - Universitat Basel , Wiley Online Library on [16/01/2026]. See the Terms and Conditions (https://onlinelibrary.wiley.com/terms-and-conditions) on Wiley Online Library for rules of use; OA articles are governed by the applicable Creative Commons License

reaching 2.3 g N m^{-3} and 520 mg P m^{-3}, respectively (Buergi and Stadelmann 2000; Müller et al. 2021). Although mitigation strategies have significantly reduced P inputs, lowering its concentrations to 24 mg P m^{-3} nowadays, the lake remains eutrophic (Müller et al. 2021). Due to the persistently high levels of nutrient inputs, high OM fluxes, and consequent development of seasonal anoxia in the water column, the lake has been continuously oxygenated/aerated artificially and systematically monitored since the 1980s (Gächter and Wehrli 1998; Buergi and Stadelmann 2000; Müller et al. 2021). Previous studies have demonstrated the critical role of sedimentary denitrification in effectively eliminating fixed N from external loading (Müller et al. 2021; Baumann et al. 2022, 2024).

Sample collection and processing

As part of the ongoing monitoring program, CTD and O_2 profiles were obtained monthly/bimonthly between January 2021 and March 2022. These profiles were used to assess the lake's stratification dynamics and to confirm seasonal trends of the physicochemical conditions in the water column. In addition, discrete water samples were collected using a 5-L Niskin bottle at the deepest site (66 m) at 12 to 15 different depths (2.5–20 m depth intervals) across the full water column, to measure dissolved inorganic nitrogen (DIN) concentrations (15 depths, as part of the monitoring), N isotopes and nitrification rates (12 and 7 depths, respectively, during five additional samplings). In March 2022, water samples were also collected from the lake's main tributaries and the outflow. For DIN concentrations and isotope analyses, roughly 60 mL of sample were collected from the outlet of the Niskin bottle, filtered through pre-rinsed syringe filters (0.22 μm, PVDF), and stored in polypropylene tubes at −20°C. For N_2O concentration and isotope measurements, 160 mL glass serum bottles were filled with gas-tight tubing (bubble-free and with one to two times overflow) from the Niskin bottle, fixed with either 0.1 mL saturated $HgCl_2$ or 3 mL 10 M NaOH, and stored at room temperature until analysis. For nitrification rate measurements, bubble-free water samples (with two times overflow) were collected in pre-autoclaved 250 mL glass serum bottles, containing magnetic stir bars. The bottles were immediately crimped and stored in an ice-box until further processing.

DIN concentrations, nitrate isotopic composition, and fractionation

Monthly/bimonthly [NH_4^+] and [NO_3^-] were measured at the *Dienststelle Lebensmittelkontrolle und Verbraucherschutz* facilities (Lucerne, CH). Briefly, [NO_3^-] was quantified by ion chromatography using a conductivity detector (LOQ: 1 mg NO_3^- L^{-1}). [NH_4^+] was quantified using the Berthelot reaction, with spectrophotometric detection at 690 nm (LOQ: 0.01 mg NH_4^+ L^{-1}). Prior to isotopic analyses, [NO_2^-] was measured spectrophotometrically employing the Griess method, which relies on the reaction with SAN and NED (LOQ: 0.5 μM) (Pai et al. 1990). [NO_x] (i.e., [NO_3^-] plus [NO_2^-]) was determined by reduction to NO using V(III) and subsequent chemiluminescence detection of NO (LOQ: 0.5 μM) (Wenk et al. 2014). Since [NO_2^-] consistently accounted for less than 1% of [NO_x], it was not removed. Therefore, the N isotopic compositions of NO_x and NO_3^- can be considered equivalent.

The NO_3^- N and O isotopic composition was determined using the denitrifier method. Briefly, NO_3^- was quantitatively converted to N_2O by *Pseudomonas aureofaciens* bacteria lacking the N_2O reductase enzyme (Sigman et al. 2001; Casciotti et al. 2002). The obtained N_2O was purified and cryo-concentrated using a custom purge-and-trap system before analysis by continuous-flow isotope ratio mass spectrometer (Delta V Plus, Thermo Fisher Scientific) (McIlvin and Casciotti 2010). Isotopic ratios were calibrated against international NO_3^- standards IAEA-N3 ($\delta^{15}N = 4.7‰$, $\delta^{18}O = 25.6‰$) and USGS34 ($\delta^{15}N = 1.8‰$, $\delta^{18}O = 27.9‰$), and an internal standard (UBN-1: $\delta^{15}N = 14.15‰$, $\delta^{18}O = 25.7‰$). Results were reported as ‰-deviation relative to international N (AIR) and O (Vienna Standard Mean Ocean Water) standards (Wenk et al. 2016; Xu et al. 2016; Sigman and Fripiat 2019). Isotopic compositions were calculated as $\delta = (R_{sample}/R_{standard} - 1) \times 1000$, where R is the ratio of heavy to light isotopologues (e.g., $^{15}N/^{14}N$ or $^{18}O/^{16}O$) in the sample or in the standard, respectively. Blank contributions accounted for less than 1% of the target sample size. The standard deviation for triplicate measurements was better than 0.3‰ for both $\delta^{15}N$ and $\delta^{18}O$. In the context of interpreting $\delta^{18}O$-NO_3^- and correcting NO_3^--derived $\delta^{18}O$-N_2O values, the $\delta^{18}O$-H_2O from the water column was measured using laser absorption spectroscopy (LWIA-24-EP), with a standard deviation of 0.10‰.

N and O isotope effects, $^{15}\varepsilon$ and $^{18}\varepsilon$, associated with net NO_3^- consumption were approximated using the Rayleigh model, assuming a closed system and constant fractionation. The isotope effects are defined as $\varepsilon = (^{L}k/^{H}k - 1) \times 1000$, where ^{L}k and ^{H}k represent the reaction rates of the light and heavy isotopologues, respectively. The isotope effect is calculated from the following equation:

$$\delta_S = \delta_{S,0} - \varepsilon \times \ln(f) \quad (1)$$

where δ_S and $\delta_{S,0}$ denote the isotopic compositions of the remaining and the source substrate, respectively, and f is the fraction of residual substrate ($[NO_3^-]_S/[NO_3^-]_{S,0}$). For each sampled month, for $[NO_3^-]_{S,0}$ and $\delta_{S,0}$, concentration and isotope values were adopted from the 30 m-depth sample, as measurements at this depth exhibited minimal seasonal variation (Wenk et al. 2014).

We acknowledge that the co-occurrence of NO_3^- consumption (assimilation/denitrification) and (re)generation processes violates the Rayleigh-model assumptions (i.e., single process, closed system with no substrate production). Hence, the calculated $^{15}\varepsilon$ and $^{18}\varepsilon$ values should be considered community isotope effects, potentially integrating the effects of multiple processes. From a more positive perspective, deviation from

19395590, 2026, 1, Downloaded from https://aslopubs.onlinelibrary.wiley.com/doi/10.1002/lno.70281 by Moritz F. Lehmann - Universitat Basel , Wiley Online Library on [16/01/2026]. See the Terms and Conditions (https://onlinelibrary.wiley.com/terms-and-conditions) on Wiley Online Library for rules of use; OA articles are governed by the applicable Creative Commons License

true Rayleigh behavior (i.e., deviation from linearity in the correlation between $\delta^{15}N$ or $\delta^{18}O$ and $\ln(f)$) can provide diagnostic insight into gross NO_3^- regeneration by nitrification in the water column.

Finally, NO_3^- isotope anomalies, $\Delta(15,18)$, were used to quantify the degree of decoupling in dual NO_3^- N and O isotope measurements:

$$\Delta(15,18) = \left(\delta^{15}N - \delta^{15}N_{ref}\right) - \left({}^{15}\varepsilon/{}^{18}\varepsilon\right) \times \left(\delta^{18}O - \delta^{18}O_{ref}\right) \quad (2)$$

where ${}^{15}\varepsilon/{}^{18}\varepsilon \sim 1$ (Sigman et al. 2005; Casciotti et al. 2008), and the reference isotopic compositions ($\delta^{15}N_{ref}$ and $\delta^{18}O_{ref}$) were based on the NO_3^- isotopic composition at 30 m water depth.

N_2O concentrations, isotope ratios, and fluxes

The N_2O concentrations, bulk isotopic composition ($\delta^{15}N_{bulk}$ and $\delta^{18}O$), and SP were determined using a custom-built purge-and-trap system coupled via a ConFlo IV to an isotope ratio mass spectrometer (Thermo, Delta V). Briefly, using helium as a carrier gas, sample N_2O was purged from the 160 mL sample vials, cryo-concentrated, and purified in a GC column (RT®-Q-BOND, 30 m, RESTEK, 25°C). The m/z ratios 30, 31, 44, 45, and 46 were detected simultaneously. The measured N_2O isotope ratios were corrected for isotope scrambling in the ion source, calibrated using three isotopic mixtures of N_2O in synthetic air (Frame and Casciotti 2010; Kelly et al. 2024), and converted to $\delta^{15}N\text{-}N_2O_{bulk}$ (referenced to AIR) and $\delta^{18}O\text{-}N_2O$ (referenced to V-SMOW). N_2O concentrations were calculated based on the slope of the peak areas ($m/z = 44 + 45 + 46$) resulting from variable injection volumes of known N_2O reference gas volumes, with a precision of 2 nM. The sample reproducibility for duplicate measurements was 2‰ for SP, 0.6‰ for $\delta^{15}N\text{-}N_2O_{bulk}$, 1.3‰ for $\delta^{18}O\text{-}N_2O$. To identify potential N_2O source(s) in the water column, measured N_2O isotope ratios (SP and bulk) were compared with N_2O isotope mixing endmembers (Yu et al. 2020). The measured values were background-corrected for the annual average isotopic composition of the respective precursor compounds, that is, $\delta^{18}O\text{-}H_2O$ (− 8.2‰), and $\delta^{15}N\text{-}NO_3^-$ (12.1‰) or $\delta^{15}N\text{-}NH_4^+$ for reductive and oxidative N_2O production, respectively. The $\delta^{15}N\text{-}NH_4^+$ value was approximated using the $\delta^{15}N_{Sinking\ PON}$ value (12.5‰), thereby assuming negligible isotope fractionation during PON remineralization to NH_4^+.

Air-lake N_2O fluxes were estimated using surface-water [N_2O] and temperature data (2.5 m depth), atmospheric [N_2O] (obtained from https://www.n2olevels.org/; accessed in November 2024), and wind speed data from the nearby Mosen weather station (Kelly et al. 2021).

Nitrification rates

To quantify nitrification rates, ${}^{15}NH_4^+$ addition experiments were performed following an established protocol (Holtappels et al. 2011). The sampled water in 250 mL serum bottles was amended with ${}^{15}N$-labeled NH_4^+ to a final concentration of 5 μM, using a Hamilton glass syringe filled with a tracer stock solution (200 mM). Unlike in the original protocol (Holtappels et al. 2011), our experiments were not subject to helium purging, in order to maintain oxic conditions throughout the experiments, consistent with the in situ conditions of Lake Baldegg's water column. After adding ${}^{15}NH_4^+$, the bottles were mixed on a stir plate, and aliquoted into 12 mL exetainers (Labco, UK). The experiments were terminated at designated time points (0, 6, 12, 24, and 36 h), by first creating a 2 mL helium headspace, followed by the addition of 100 μL $ZnCl_2$ solution (50% w/v). Fixed samples were stored at room temperature in the dark and analyzed within 6 months.

For the determination of ${}^{15}NH_4^+$ consumption, NH_4^+ was converted to N_2 gas using the alkaline-hypobromite method (Jensen et al. 2011; Robertson et al. 2016). The NH_4^+-derived ${}^{14}N{}^{15}N$ in the exetainer headspace was measured by GC-IRMS analysis (Isoprime, Manchester, UK), and its decrease over time was determined. The slope of the linear regression was used to estimate the ${}^{15}NH_4^+$ turnover rates, and the standard error was calculated from the deviation in the regression slope across the five time points. To ensure that the rates were significantly different from zero, a one-tailed *t*-test (95% confidence level) was applied (Thamdrup and Dalsgaard 2002). Regeneration of NH_4^+ was not explicitly considered in the uptake rate calculations, as the potential for dilution of the ${}^{15}N$ tracer was minimal. Background NH_4^+ concentrations in the water column were consistently low (averaging ~ 1 μM across depths; Fig. 2), meaning that the added ${}^{15}NH_4^+$ tracer made up the vast majority of the available NH_4^+ pool in our incubations. As such, we are confident that uptake rates were not significantly underestimated due to isotope dilution.

Statistical analyses

The seasonal variability of all measured parameters (nitrification rates, NO_3^- and N_2O concentrations and isotope ratios) from the 2021/2022 sampling campaign, was assessed using ANOVA. Post hoc comparisons were conducted using Tukey's HSD test at a 95% confidence level to identify significant differences. Differences in nitrification rates between the epilimnion and hypolimnion were tested using a two-tailed *t*-test (95% confidence level). Correlations among all investigated variables were assessed using the Spearman's rank correlation method, with significance determined at a 95% confidence level. All statistical analyses were performed in RStudio.

All field data and isotope mass-balance model outcomes (below) are available on Zenodo (https://doi.org/10.5281/zenodo.15229683).

Isotope mass-balance model

To investigate the expected effects of N consumption and regeneration on the water column $\delta^{15}N\text{-}NO_3^-$ and to assess the role of nitrification in sustaining NO_3^- loss, a simplified

19395590, 2026, 1, Downloaded from https://aslopubs.onlinelibrary.wiley.com/doi/10.1002/lno.70281 by Moritz F. Lehmann - Universitat Basel , Wiley Online Library on [16/01/2026]. See the Terms and Conditions (https://onlinelibrary.wiley.com/terms-and-conditions) on Wiley Online Library for rules of use; OA articles are governed by the applicable Creative Commons License

mass-balance isotope modeling approach was applied to the full water column (*Box A*) during the mixed period (March–May), and separately to the epilimnion (*Box B*) and the hypolimnion (*Box C*) during the stratification period (July–November) (Supporting Information Fig. S1). Each compartment was treated as a homogenized box, as described for previously employed models (Bourbonnais et al. 2009). External N inputs were assumed to mix uniformly across the entire water column (*Box A*) or only in the epilimnion (*Box B*). The hypolimnion (*Box C*) was considered a closed system during stratification, with negligible exchange with the epilimnion. A detailed model description, with all relevant processes, equations, and assumptions is provided in the Supporting Information.

Results

Seasonal water column dynamics and hydrochemistry

Epilimnion (0–15 m)

Thermal stratification consistently developed between June and October (Fig. 1a). Increased algal productivity during this period reduced [NO_3^-] from approximately 145 μM to 115–120 μM (Fig. 1c). Although NO_3^- is rarely bio-limiting in Swiss meso- to eutrophic lakes (Lehmann et al. 2004a) and NO_3^- utilization in Lake Baldegg was less pronounced than in other Swiss lakes (Lehmann et al. 2004b; Tadonleke et al. 2009; Müller et al. 2021), the seasonal variability, characterized by a summer [NO_3^-] drawdown, was significant ($p < 0.01$). Following algal growth and OM production in spring/early summer, OM remineralization led to strong O_2 consumption near the pycnocline (10–15 m), creating suboxic, and ultimately anoxic conditions between September and November (0–30 μM O_2) (Fig. 1b). Transient NH_4^+ accumulation (up to 12 μM at 10 m) occurred in August, while [NH_4^+] otherwise remained below 2 μM (Fig. 1d).

Hypolimnion (15–66 m)

Hypolimnetic anoxia, caused by OM decomposition, was mitigated by artificial oxygenation using pure O_2 (March to November) (Buergi and Stadelmann 2000), and by aeration (November to March). Nonetheless, hypoxic conditions developed near the sediments (60–65 m) between June and November, with [O_2] dropping to 31 μM in September (Fig. 1b). Simultaneously, [NO_3^-] slightly decreased to 117–129 μM, and [NH_4^+] peaked at 9.2–10.4 μM (Fig. 1c,d).

Seasonal transition: Stratified vs. mixed

The annual overturn in December/January homogenized the water column, exhibiting uniform concentrations of 266 μM O_2, 143 μM NO_3^- and 0.4–1.2 μM NH_4^+ (Fig. 1b,c). Hereafter, the stratified season refers to June–November, whereas the December–May period represents the mixed season, which started with the water column aeration in November. The [NO_3^-] in the samples collected specifically for DIN isotope analyses (Fig. 2a) closely matched the concentrations obtained through the routine monitoring program, reflecting identical temporal and spatial dynamics. These results are discussed further in the context of NO_3^- isotopes. As [NO_2^-] remained below 1% of [NO_3^-], NO_2^- data will not be discussed further.

N_2O dynamics

Between May and September, epilimnetic [N_2O] remained close to air equilibration levels (10.8 nM ± 0.8 nM), with slight oversaturation (103%–127%) resulting in low net N_2O emissions to the atmosphere (0.06–0.26 μmol m^{-2} d^{-1}) (Supporting Information Table S2). However, in November, [N_2O] peaked in the epilimnion (100 nM), leading to strong N_2O oversaturation (845 ± 17%) and a high flux (3.52 ± 0.08 μmol m^{-2} d^{-1}) (Supporting Information Table S2). In the hypolimnion, N_2O accumulated progressively during stratification, reaching roughly 60 nM in autumn (Fig. 2e).

Nitrate N and O isotope dynamics (and apparent isotope effects)

In the epilimnion, small but statistically significant ($p < 0.05$) [NO_3^-] fluctuations were accompanied by systematic variations in δ^{15}N- and δ^{18}O-NO_3^- (Fig. 2). Depth-integrated δ^{15}N-NO_3^- data exhibited significant seasonality in the epilimnion ($p < 0.01$), increasing as stratification progressed from 12.3‰ in March to 13.6‰ in November at 2.5 m (Fig. 2b). The apparent N isotope fractionation factor for net NO_3^- consumption, $^{15}\varepsilon$, rose from 3.4‰ in July to 5.7‰ in September and to 9.2‰ in November (Supporting Information Fig. S2a), consistent with values for NO_3^- assimilation (4–10‰) (Botrel et al. 2017). The δ^{18}O-NO_3^- also increased during stratification (Fig. 2c), with apparent community $^{18}\varepsilon$ values of 11.0–12.1‰ in July–November. In contrast, no evident (N or O) isotope enrichment was detected in March–May. Most δ^{15}N-NO_3^- and δ^{18}O-NO_3^- values were within the range defined by the tributaries, and comparable to those of the outflow (Fig. 3a). Deviations from a 1 : 1 N-vs.-O isotope enrichment ratio (i.e., $\Delta\delta^{18}O : \Delta\delta^{15}N = 1.5$ in July and 1.73 in September/November) (Fig. 3b) produced NO_3^- isotope anomalies, Δ(15,18) (Eq. 2) (Sigman et al. 2005; Bourbonnais et al. 2009), as low as −1.5 during stratification. In March–May, Δ(15,18) remained close to zero (Fig. 2d; Supporting Information Table S4).

In the hypolimnion, seasonal changes in δ^{15}N-NO_3^- were subtle, and there was minimal depth-dependent variation in δ^{18}O-NO_3^- (Fig. 2b,c). The relatively weak ^{15}N and ^{18}O enrichments (δ^{15}N-NO_3^-: 11.1‰ in September to 12.3‰ in March at 63 m; δ^{18}O-NO_3^-: 0.6–0.8‰ in September–October to 2.2–2.5‰ in March–May) precluded the calculation of apparent community N and O isotope effects (Supporting Information Fig. S2b). Additionally, no clear correlation between δ^{15}N-NO_3^- and δ^{18}O-NO_3^- was observed in the dual isotope plot (Fig. 3b).

N_2O isotope dynamics

Excluding November 2021, epilimnetic N_2O SP values closely resembled atmospheric values (15–20‰) (Fig. 2e,f). During stratification, δ^{15}N-N_2O increased toward the surface

19395590, 2026, 1, Downloaded from https://aslopubs.onlinelibrary.wiley.com/doi/10.1002/lno.70281 by Moritz F. Lehmann - Universitat Basel , Wiley Online Library on [16/01/2026]. See the Terms and Conditions (https://onlinelibrary.wiley.com/terms-and-conditions) on Wiley Online Library for rules of use; OA articles are governed by the applicable Creative Commons License

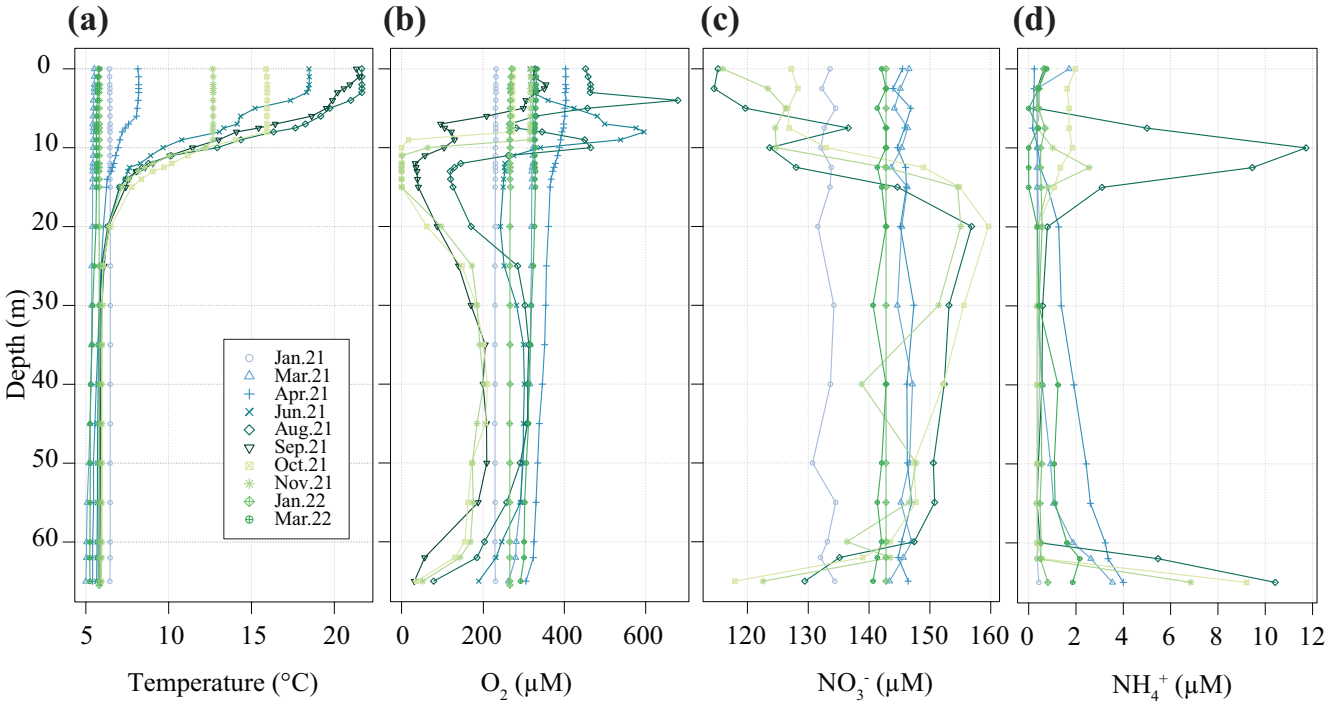

Fig. 1. Water column vertical profiles for (**a**) temperature (°C), (**b**) O_2 (μM), (**c**) NO_3^- (μM), and (**d**) NH_4^+ (μM) for January 2021–March 2022.

(3–4‰ enrichment), whereas no discernible ^{18}O enrichment was observed (Fig. 2g,h). Significant seasonality ($p < 0.01$) in all epilimnetic N_2O isotopic parameters was primarily ascribed to the November data, when a transient [N_2O] buildup (100 nM) coincided with sharp increases in SP (45‰) and $\delta^{18}O$-N_2O (60‰), together with a $\delta^{15}N_{bulk}$-N_2O minimum of −3.8‰.

Hypolimnetic [N_2O] also varied seasonally ($p < 0.01$). During stratification, N_2O accumulated with depth, reaching up to 60 nM at 63 m in September (Fig. 2e), and exhibited SP values consistently above 30‰, yet without systematic seasonality (Fig. 2f). Both $\delta^{15}N$-N_2O and $\delta^{18}O$-N_2O increased with depth, reaching 2‰ and 55‰, respectively, at 63 m (Fig. 2g,h), though no gradual seasonal trend was evident.

Coupled N-vs.-O N_2O isotope signatures were assessed separately for the epilimnion and the hypolimnion (Supporting Information Fig. S3a,b). In the epilimnion, the $\delta^{18}O : \delta^{15}N$ slope increased from 0.35 in July to 0.60 in September ($R^2 = 0.86$ and 0.57, respectively), indicating stronger N than O heavy-isotope enrichment (Supporting Information Fig. S3a). A strong inverse correlation was observed in November (ratio of −1.92, $R^2 = 0.99$). In the hypolimnion, clear $\delta^{18}O$ vs. $\delta^{15}N$ correlations were found only in May (2.30, $R^2 = 0.97$) and July (0.79, $R^2 = 0.95$).

A comparison with potential N_2O mixing endmembers placed N_2O data between atmospheric and nitrification-derived values (Fig. 4). In the SP-vs.-$\delta^{15}N$ plot (Fig. 4a), epilimnetic data clustered near atmospheric values, while hypolimnetic values showed more nitrification-driven signatures. This pattern was less obvious in the SP vs. $\delta^{18}O$ plot, as $\delta^{18}O$-N_2O values were shifted to higher values than expected for an atmospheric–nitrification mixed signal (Fig. 4b). Notably, the November epilimnetic N_2O data stood out across the dataset, displaying elevated SP and $\delta^{18}O$-N_2O values.

Nitrification rates

Nitrification was observed year-round, with no significant seasonality in absolute nitrification rates in either the epilimnion or hypolimnion ($p > 0.05$) (Fig. 5a). However, depth-integrated nitrification rates were significantly higher in the hypolimnion than in the epilimnion in July and September, before declining below 500 μmol m^{-2} d^{-1} in November (Fig. 5b). The most pronounced difference occurred in September, when epilimnetic nitrification rates remained consistently below 40 nM d^{-1}, while hypolimnetic rates exceeded 60 nM d^{-1} (Fig. 5a).

Isotope mass-balance model

Our data suggest minimal NO_3^- consumption in Lake Baldegg, as only subtle changes in [NO_3^-] and $\delta^{15}N$-NO_3^- were observed. However, earlier research reported high N removal, with up to 66% of the annual N load removed via algal NO_3^- uptake and OM production, combined with subsequent N export/burial and heterotrophic denitrification (Müller et al. 2021). Given our evidence of active nitrification throughout the water column (Fig. 5), we argue that the minimal changes in [NO_3^-] and $\delta^{15}N$-NO_3^- reflect a near-balance

19395590, 2026, 1, Downloaded from https://aslopubs.onlinelibrary.wiley.com/doi/10.1002/lno.70281 by Moritz F. Lehmann - Universitat Basel , Wiley Online Library on [16/01/2026]. See the Terms and Conditions (https://onlinelibrary.wiley.com/terms-and-conditions) on Wiley Online Library for rules of use; OA articles are governed by the applicable Creative Commons License

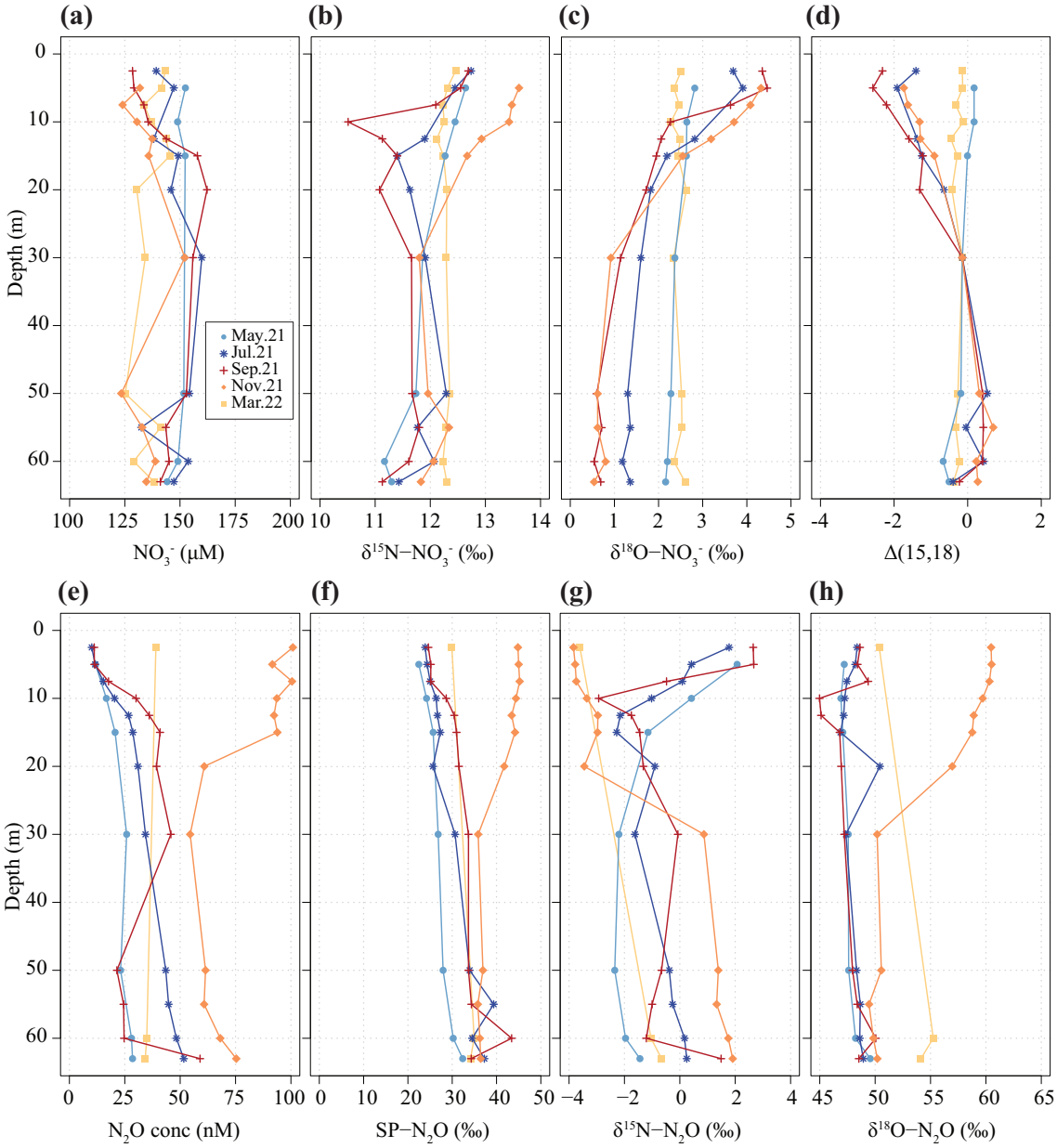

Fig. 2. Water column vertical profiles for (**a**) NO_3^- concentrations (in μM), (**b**) $\delta^{15}N\text{-}NO_3^-$ (in ‰), (**c**) $\delta^{18}O\text{-}NO_3^-$ (in ‰), (**d**) NO_3^- isotope anomalies ($\Delta(15,18)$), (**e**) N_2O concentrations (in nM), (**f**) N_2O site preference (in ‰), (**g**) $\delta^{15}N\text{-}N_2O_{bulk}$ (in ‰), and (**h**) $\delta^{18}O\text{-}N_2O$ (in ‰) for all sampled months in 2021/2022.

between NO_3^- consumption and regeneration, combined with external N inputs. To investigate this, we combined nitrification rate measurements with DIN data in an isotope mass balance (*see* Supporting Information for details). This framework enabled us to discern the roles of nitrification and external loading in sustaining NO_3^- assimilation and denitrification, as well as their impact on measured $[NO_3^-]$ and $\delta^{15}N\text{-}NO_3^-$ (Supporting Information Table S3; Fig. 6). Our objective was to evaluate whether the NO_3^- isotope method, successfully applied in marine systems to quantify nitrification under net N-consuming conditions (Sigman et al. 2005), yields meaningful results in a eutrophic lake with substantial external N inputs.

Box A: Entire water column during the mixed season - External N inputs were homogeneously distributed throughout the water column, adding 340 μM NO_3^- with a $\delta^{15}N\text{-}NO_3^-$ = 10.4‰ to the system (Fig. 6a; Supporting Information Table S3). This increased the lake's internal $[NO_3^-]$ to 484 ± 4 μM and lowered $\delta^{15}N\text{-}NO_3^-$ from 12.1‰ to 10.9 ± 0.1‰. The role of internal N cycling was then evaluated, revealing that depth-integrated nitrification rates

19395590, 2026, 1, Downloaded from https://aslopubs.onlinelibrary.wiley.com/doi/10.1002/lno.70281 by Moritz F. Lehmann - Universitat Basel , Wiley Online Library on [16/01/2026]. See the Terms and Conditions (https://onlinelibrary.wiley.com/terms-and-conditions) on Wiley Online Library for rules of use; OA articles are governed by the applicable Creative Commons License

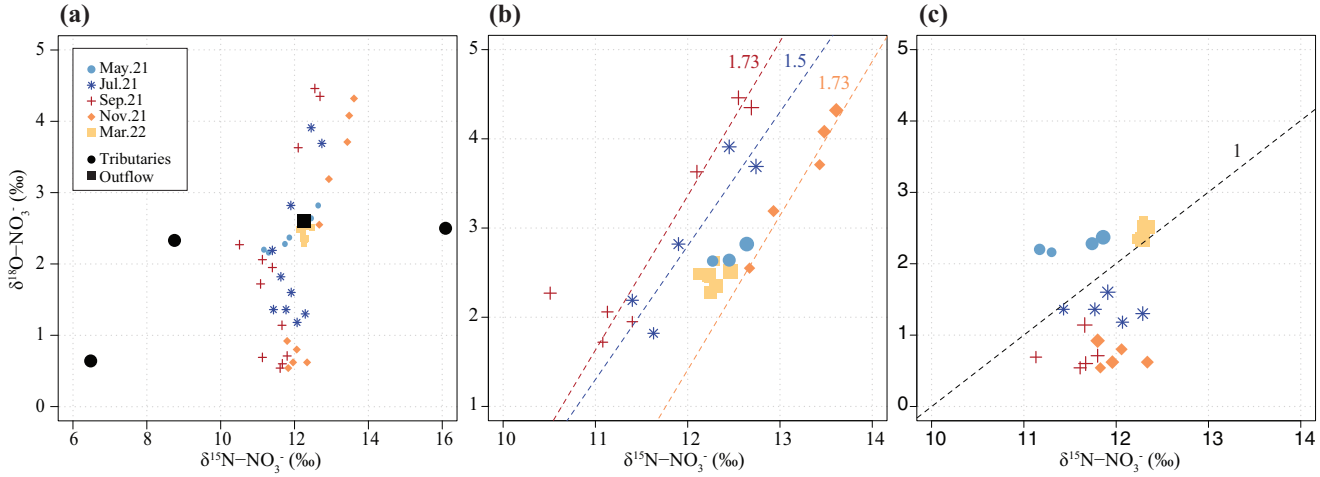

Fig. 3. Dual N-vs.-O NO_3^- isotopes for (**a**) complete water column, tributaries and outflow, (**b**) the epilimnion and (**c**) the hypolimnion for all sampled months in 2021/2022. Symbol size in (b) and (c) decreases with increasing water-column depth. Dashed lines represent observed $\Delta\delta^{18}O : \Delta\delta^{15}N$ during stratification, with the corresponding slope coefficients reported for each month (b). For comparison, the black dashed line in (c) represents the canonical $\Delta\delta^{18}O : \Delta\delta^{15}N$ slope for a purely denitrifying system.

contributed $86 \pm 8\ \mu M$ ($[NO_3^-]_{Nitrification}$), decreasing $\delta^{15}N\text{-}NO_3^-$ to 9.2 ± 0.4‰. Consumption of NO_3^- was likely driven by a combination of NO_3^- assimilation (although significant algal blooms were reported to start only in June [Müller et al. 2021]) and benthic denitrification, as oxic conditions inhibited water column denitrification at that time (Fig. 1b). Consumed NO_3^- was quantified at $226 \pm 5.4\ \mu M$ when nitrification was neglected, and at $312 \pm 9.7\ \mu M$ when nitrification was considered, indicating that nitrification sustained $27.3 \pm 3.4\%$ of total NO_3^- consumption (i.e., $[NO_3^-]_{Combined}$). Average consumption rates were 107.5 ± 6.6 nM d^{-1}. The combined effects of nitrification and NO_3^- consumption could result in $\delta^{15}N\text{-}NO_3^-$ values ranging from 8.6‰ to 13.7‰, depending on the chosen N isotope effects. Given $^{15}\varepsilon_{Nitrification} = 15 \pm 3$‰ and the quantified $[NO_3^-]$, a community N isotope effect $^{15}\varepsilon_{Consumption}$ of 3.6 ± 0.5 ‰ would explain the observed $\delta^{15}N\text{-}NO_3^-$.

Box B: Epilimnion during stratification - External N loadings mixed exclusively within the epilimnion (i.e., $[NO_3^-]_{External} = 840\ \mu M$), increasing $[NO_3^-]$ from $156 \pm 4\ \mu M$ to $996 \pm 4\ \mu M$ and lowering its $\delta^{15}N\text{-}NO_3^-$ from 11.8 ± 0.1‰ to 10.7 ± 0.0‰ (Fig. 6b; Supporting Information Table S3). Nitrification (depth-integrated) added only $33 \pm 3\ \mu M$ NO_3^- to the system, subtly decreasing $\delta^{15}N\text{-}NO_3^-$ to 10.2 ± 0.1‰.

Assimilation removed $578 \pm 5\ \mu M$ NO_3^- if nitrification-derived NO_3^- was neglected, and $610 \pm 6\ \mu M$ NO_3^- if NO_3^- regeneration via nitrification was accounted for. The combined effects of nitrification and assimilation would explain $\delta^{15}N\text{-}NO_3^-$ values of 14.7 ± 2.8‰, encompassing the measured $\delta^{15}N\text{-}NO_3^-$ (12.4 ± 0.7‰; Fig. 6b). Yet, nitrification sustained only $5.3 \pm 0.7\%$ of total NO_3^- assimilation, as external inputs served as the primary NO_3^- source. The average consumption rates were 297.2 ± 2.5 nM d^{-1}.

Box C: Hypolimnion during stratification - Isolated from external sources, hypolimnetic N cycling was driven by nitrification and denitrification (both sedimentary and water column). Nitrification added $102 \pm 14\ \mu M$ NO_3^-, reducing $\delta^{15}N\text{-}NO_3^-$ from 11.8 ± 0.1‰ to 8.1 ± 2.3 ‰ (Fig. 6c; Supporting Information Table S3). Calculated denitrification removed little NO_3^- if nitrification was neglected ($[NO_3^-]_{Consumption} = 14 \pm 5\ \mu M$), and significantly more when nitrification-derived NO_3^- was accounted for ($116 \pm 16\ \mu M$), indicating that nitrification sustained most of the NO_3^- consumption ($81.6 \pm 18.5\%$). Average consumption rates were 44.3 ± 22.1 nM d^{-1}. Notably, concentration-based measurements alone would have underestimated NO_3^- consumption, as concurrent NO_3^- production and consumption effectively balanced each other.

The measured $\delta^{15}N\text{-}NO_3^-$ (11.8 ± 0.3‰) fell within the model-derived community $\delta^{15}N\text{-}NO_3^-$ range (8.1 ± 2.3‰ to 22.5 ± 5.1‰) obtained considering either sedimentary or water column denitrification (endmember N isotope effects: $^{15}\varepsilon_{Denitrification} = 0$‰ vs. 25‰). Specifically, the measured $\delta^{15}N\text{-}NO_3^-$ can be explained with a N isotope effect for community denitrification, $^{15}\varepsilon_{Denitrification}$, of 6.7 ± 1.5‰ (for a given $^{15}\varepsilon_{Nitrification} = 15 \pm 3$‰). The calculated $^{15}\varepsilon_{Denitrification}$ increased slightly as stratification progressed (6.0 ± 1.6‰, 6.4 ± 1.5‰ and 7.6 ± 1.4‰ in July, September and November, respectively), coinciding with suboxia, and eventually anoxia, in the water column (Fig. 1b). This favored water column denitrification, known to express a higher $^{15}\varepsilon_{Denitrification}$. Using the two $^{15}\varepsilon_{Denitrification}$ endmembers, 0‰ for sedimentary and 25‰ for water column denitrification, the latter was estimated to contribute $24.1 \pm 6.2\%$, $25.6 \pm 6.0\%$ and $30.2 \pm 5.7\%$ to the total (i.e., community) denitrification in July, September and November, respectively (Fig. 6).

19395590, 2026, 1, Downloaded from https://aslopubs.onlinelibrary.wiley.com/doi/10.1002/lno.70281 by Moritz F. Lehmann - Universitat Basel , Wiley Online Library on [16/01/2026]. See the Terms and Conditions (https://onlinelibrary.wiley.com/terms-and-conditions) on Wiley Online Library for rules of use; OA articles are governed by the applicable Creative Commons License

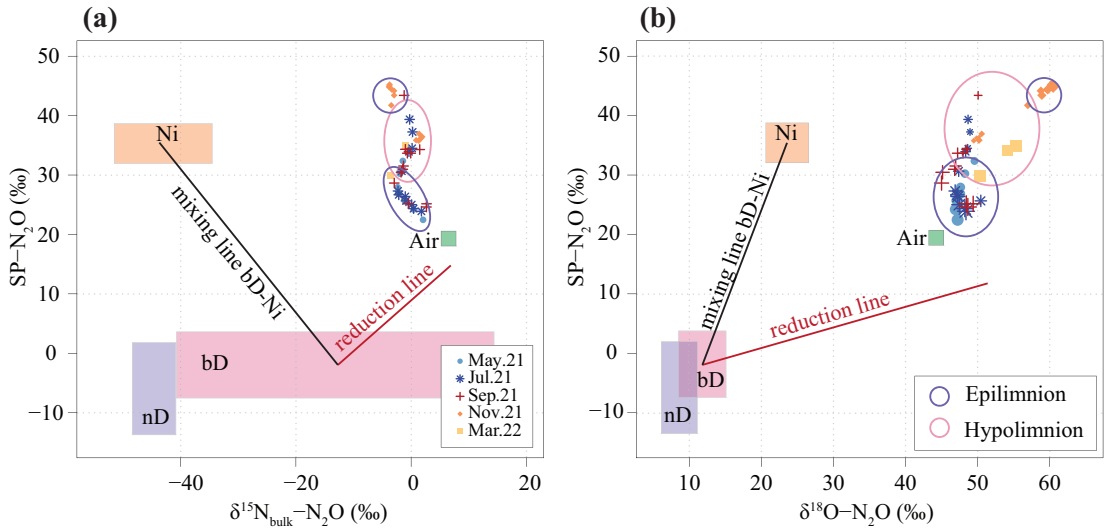

Fig. 4. Dual N_2O isotope plots across the full water column: (**a**) SP vs. $\delta^{15}N_{bulk}$-N_2O, and (**b**) SP vs. $\delta^{18}O$-N_2O. Data for the epilimnion and hypolimnion are circled in blue and pink, respectively. N_2O source endmembers are indicated for nitrification (Ni, orange), bacterial denitrification (bD, pink) and nitrification–denitrification (nD, purple), alongside the theoretical reduction line (red) and the mixing line between nitrification and bacterial denitrification (black), as detailed by (Yu et al. 2020). Values for atmospheric air are represented by the green square. Measured values are background-corrected for the annual average isotopic composition of the respective precursor compounds, that is, $\delta^{18}O$-H_2O (−8.2‰), and $\delta^{15}N$-NO_3^- (12.1‰) or $\delta^{15}N$-NH_4^+ (approximated using the $\delta^{15}N_{Sinking\ PON}$ value, 12.5‰) for reductive and oxidative N_2O production, respectively.

Discussion

Quantifying the importance of nitrification in sustaining NO_3^- consumption

Nitrification and external N loading as NO_3^- sources

The combination of Rayleigh-derived isotope effects, dual N and O NO_3^- isotope signatures, and isotope mass balancing, successfully employed in marine environments (Sigman et al. 2005), proved challenging in Lake Baldegg due to the substantial external N inputs. Water column $\delta^{15}N$-NO_3^- and $\delta^{18}O$-NO_3^- values mostly resembled values from tributaries (Fig. 3a; Supporting Information Table S5), consistent with manure-derived NO_3^- ($\delta^{15}N$-NO_3^- = +10‰ to +20‰; $\delta^{18}O$-NO_3^- = −15‰ to +15‰ [Kendall et al. 2007]). Atmospheric deposition ($\delta^{15}N$-NO_3^- = −15‰ to +15‰ and $\delta^{18}O$-NO_3^- = +14‰ to +75‰ [Xu et al. 2016]), may also affect water column NO_3^- isotopic signatures, though it was not quantified in this study. Additionally, N_2 fixation could add NO_3^- with low $\delta^{15}N$ (Yang et al. 2022), but it is minimal in lakes with high N loading (Scott et al. 2019), and likely irrelevant at the study site, given the dominance of non-N_2-fixing cyanobacterium *Planktothrix rubescens* (Müller et al. 2021). Overall, external N loading (Müller et al. 2021) sustained 72% of NO_3^- consumption during the mixed season and up to 95% in the epilimnion during stratification.

Despite the dominance of external inputs, isotope and rate measurements confirm active nitrification, also contributing to the NO_3^- pool. Indeed, dual NO_3^- isotope ratios and isotope anomalies indicated significant NO_3^- regeneration in the epilimnion during stratification (Figs. 2d, 3b, 5). The Rayleigh-derived community N and O fractionation factors for NO_3^- consumption ($^{15}\varepsilon$ = 3.4–9.2‰ and $^{18}\varepsilon$ = 11.0–12.1‰) (Supporting Information Fig. S2) fall within previously reported ranges for NO_3^- assimilation (4–10‰) (Botrel et al. 2017). However, $\Delta\delta^{18}O : \Delta\delta^{15}N$ ratios of 1.5–1.73 indicate a disproportionately greater ^{18}O enrichment, diagnostic of nitrification (Gaye et al. 2013; Dale et al. 2022). During nitrification, incorporation of 5/6 O atoms from H_2O ($\delta^{18}O$-H_2O = −8.2‰) and 1/6 from dissolved O_2 ($\delta^{18}O$-O_2 = +23.5‰) (Casciotti et al. 2002; Frey et al. 2014) yields a theoretical $\delta^{18}O$-NO_3^- value of −2.9‰. This value is lower than the measured $\delta^{18}O$-NO_3^- (Fig. 2c), suggesting the occurrence of a ^{18}O-enriching process alongside nitrification. Furthermore, nitrification lowers the $\delta^{15}N$ of regenerated NO_3^- (Yang et al. 2022), counterbalancing the ^{15}N enrichment from NO_3^- assimilation (Wankel et al. 2007; Yang et al. 2022), and consequently, leading to $\Delta\delta^{18}O : \Delta\delta^{15}N$ ratios above 1 and negative Δ(15,18).

Hence, $\Delta\delta^{18}O : \Delta\delta^{15}N$ and Δ(15,18) values serve as indicators of NO_3^- regeneration via nitrification, provided that external NO_3^- sources are well constrained. The N isotope mass balance model effectively disentangled the contributions of external N sources and nitrification in sustaining NO_3^- consumption. These contributions, if more or less balanced by consumption processes, might go untraced by concentration measurements alone due to rapid turnover (Fig. 6; Supporting Information Table S3). Similarly, the occurrence of processes exerting low isotopic fractionation (e.g., benthic NO_3^- reduction) might be challenging to quantify from isotope measurements alone. The importance of complementing dual NO_3^- isotopes with rate measurements is evident during the mixed season, when ^{15}N and ^{18}O enrichment was absent (Fig. 2b,c), but nitrification (across the whole water column) sustained 27.3 ± 3.4% of NO_3^- consumption

19395590, 2026, 1, Downloaded from https://aslopubs.onlinelibrary.wiley.com/doi/10.1002/lno.70281 by Moritz F. Lehmann - Universitat Basel , Wiley Online Library on [16/01/2026]. See the Terms and Conditions (https://onlinelibrary.wiley.com/terms-and-conditions) on Wiley Online Library for rules of use; OA articles are governed by the applicable Creative Commons License

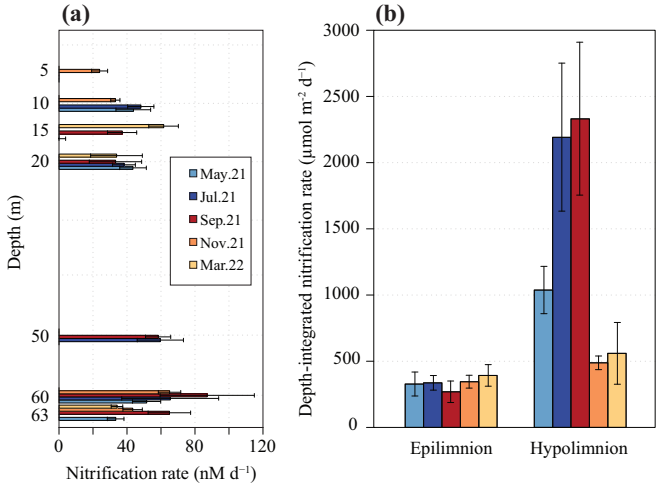

Fig. 5. (**a**) Water column nitrification rates (in nM d^{-1}) at selected depths in the epilimnion and the hypolimnion; (**b**) depth-integrated nitrification rates (in μmol m^{-2} d^{-1}) for all sampled months in 2021/2022. Error bars are plotted based on the standard error from the nitrification rate measurements.

through assimilation and benthic denitrification. During the mixed period, the isotope mass-balance model yielded a low N isotope effect of 3.6 ± 0.5‰ for net NO_3^- consumption (Fig. 6), consistent with combined contributions from assimilation ($^{15}\varepsilon \approx 5‰$) (Granger et al. 2004) and benthic denitrification ($^{15}\varepsilon \approx 0‰$) (Lehmann et al. 2007).

Hypolimnetic nitrification and its coupling with denitrification/DNRA

Hypolimnetic nitrification was sustained year-round by OM remineralization and peaked in July–November thanks to high sedimentation rates (13.03–74.69 mg N m^{-2} d^{-1}) (Müller et al. 2021). Thermal stratification isolated the hypolimnion, minimizing the influence of external inputs, and increasing the relative importance of regenerated NO_3^-. During stratification, the lack of pronounced ^{15}N and ^{18}O enrichment in the residual NO_3^- pool (Fig. 2b,c) and the absence of distinct features in the dual NO_3^- isotopes plot (Fig. 3c) and Δ(15,18) profiles (Fig. 2d), reflect rapid and closely coupled NO_3^- production and consumption, rather than a stagnant N cycle. Hypolimnetic nitrification continuously produced ^{15}N-depleted NO_3^-, "diluting" the expected ^{15}N enrichment due to water column denitrification. Additionally, low community N isotope effects of NO_3^- consumption (6.0–7.6‰) indicate that denitrification/DNRA in sediments dominates (Lehmann et al. 2004c), consistent with Müller et al. (2021) and Baumann et al. (2022, 2024).

Water column denitrification may also have contributed to hypolimnetic NO_3^- consumption (Fig. 1b). The model-derived community N isotope effect of NO_3^- consumption shifted from 6.0 ± 1.6‰ in July to 7.6 ± 1.5‰ in November, suggesting that the proportion of water column relative to sedimentary denitrification increased as stratification progressed and suboxic conditions developed, from 24.1 ± 6.2% in July to 30.1 ± 5.7% in November (Fig. 6).

Some water-column denitrification might be associated with suspended or resuspended particles (Zhou et al. 2019; Yeerken et al. 2023), as bacteria residing within anoxic microniches (Xia et al. 2017) can reduce NO_3^- even in oxic waters (Cojean et al. 2019). This is facilitated by sharp O_2 gradients within particles (Fuchsman et al. 2019), and NO_3^- supplied by particle-attached nitrifiers (Zhou et al. 2019). If NO_3^--reducing bacteria are indeed associated with resuspended particles, their activity could suppress the N isotope effect, complicating the efforts to clearly distinguish between benthic and particle-associated water-column denitrification. Consequently, the proportion of water-column denitrification estimated by our model may represent a lower bound.

N_2O dynamics and production pathways

N_2O concentrations in Lake Baldegg rank among the highest in Swiss lakes, reaching 100–140 nM (Mengis et al. 1997). At the end of stratification, N_2O fluxes into the atmosphere attained 3.52 ± 0.08 μmol m^{-2} d^{-1} (Supporting Information Table S2), driven by elevated epilimnetic [N_2O] in November (Fig. 2e). We argue that these emissions largely originate from progressive hypolimnetic N_2O accumulation during stratification, and its transfer to the epilimnion upon winter mixing. This interpretation is supported by the declining hypolimnetic [N_2O] and concurrent increases in epilimnetic [N_2O] during turnover (Fig. 2e).

Our data indicate that hypolimnetic nitrification is the primary N_2O-producing mechanism during stratification. Specifically, the high [N_2O] in September (up to 65 nM) (Fig. 2e) coincides with some of the highest nitrification rates, consistent with peak nitrification activity in late summer (Klotz et al. 2022). However, the overall relatively weak correlation between [N_2O] and nitrification rates (Supporting Information Fig. S4) suggests contributions from other processes, such as N_2O production via denitrification, nitrifier-denitrification, or N_2O reduction. Indeed, low-O_2 subsurface conditions in late summer (Fig. 1b) could promote reductive N_2O production and reduction (via denitrification). However, high N_2O SP values (> 30‰) (Fig. 2f) argue against incomplete denitrification, which typically exhibits SP values between −5‰ and 0‰ (Wenk et al. 2016). Moreover, while elevated SP and $\delta^{18}O$-N_2O values might indicate N_2O reduction (i.e., complete denitrification) (Wenk et al. 2016), $\Delta\delta^{18}O$-N_2O : $\Delta\delta^{15}N$-N_2O slopes strongly deviate from 2.5, the characteristic value for purely N_2O-reducing systems (Supporting Information Fig. S3) (Wenk et al. 2016; Liang et al. 2022). Thus, our findings indicate that oxidative production via nitrification prevails over incomplete denitrification for N_2O

19395590, 2026, 1, Downloaded from https://aslopubs.onlinelibrary.wiley.com/doi/10.1002/lno.70281 by Moritz F. Lehmann - Universitat Basel , Wiley Online Library on [16/01/2026]. See the Terms and Conditions (https://onlinelibrary.wiley.com/terms-and-conditions) on Wiley Online Library for rules of use; OA articles are governed by the applicable Creative Commons License

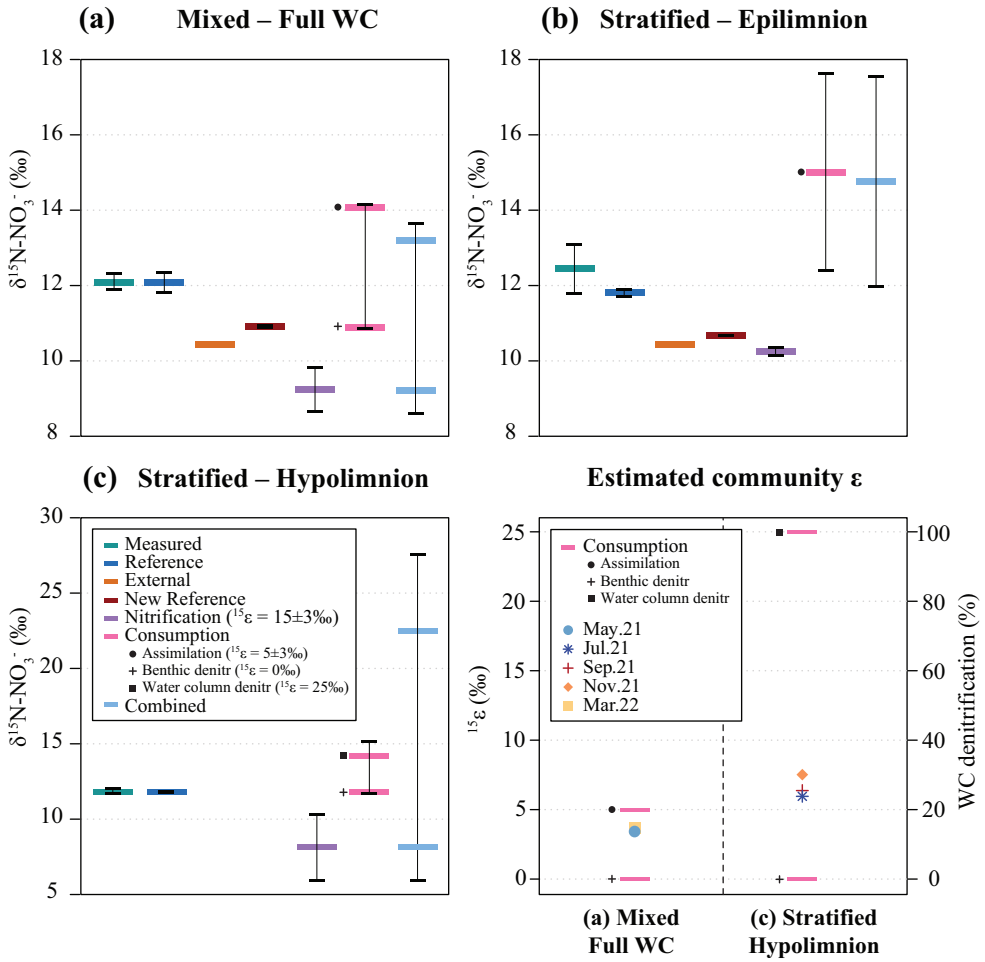

Fig. 6. Different-scenario outputs for the N isotope mass-balance model. Panels show average $\delta^{15}N\text{-}NO_3^-$ values for the different NO_3^- pools during (**a**) mixed period (March–May), full water column, (**b**) the stratified period (July–November), epilimnion, and (**c**) the stratified period, hypolimnion. Each panel includes the following NO_3^- pools: measured, reference (set at 30 m), external, new reference (i.e., resulting from the thorough mixing of external N inputs and reference), stand-alone nitrification, stand-alone consumption (assimilation and denitrification), and combined (i.e., considering both NO_3^- regeneration by nitrification and NO_3^- consumption by either assimilation or denitrification). Error bars encompass both the seasonal variability and the uncertainty associated with the chosen isotope effects: $^{15}\varepsilon_{Nitrification} = 15 \pm 3‰$, (a) $^{15}\varepsilon_{Consumption} = 0–5‰$ in the full water column during the mixed period (assuming a mixed signal of assimilation and benthic denitrification), (b) $^{15}\varepsilon_{Assimilation} = 5 \pm 3‰$ in the epilimnion, and (c) $^{15}\varepsilon_{Denitrification} = 0–25‰$ in the hypolimnion (assuming a mixed signal of benthic and water column denitrification). The estimated community $^{15}\varepsilon$ values based on the isotope mass balance for boxes (a) and (c) are reported in the lower right panel alongside the derived contribution of water column denitrification to total denitrification for the hypolimnion (c). The NO_3^--consuming processes considered for each box are: NO_3^- assimilation (circle), benthic denitrification (cross), and water column denitrification (square).

production, though the occurrence of N_2O reduction cannot be dismissed.

Upon vertical mixing, promoted by the switch from oxygenation to aeration in November, N_2O-laden hypolimnetic waters are transported to the epilimnion (Wenk et al. 2016). This is supported by decreasing hypolimnetic [N_2O], and concurrently increasing epilimnetic [N_2O] and SP values in November (Fig. 2e,f). If subsurface N_2O reduction had occurred at the end of stratification, the November [N_2O] might underestimate the originally produced [N_2O]. A previous study in Lake Alpnach (Switzerland) suggests that up to 60% of lacustrine N_2O is emitted to the atmosphere, with the rest being reduced to N_2 within the system (Mengis et al. 1997). For Lake Baldegg, precise estimates would require direct [N_2O] measurements before and after the oxygenation-to-aeration switch, but trends from earlier months (Fig. 2e) suggest that emissions may even exceed 60% of total N_2O production.

Possible effects of aeration

Artificial aeration has been widely reported to enhance nitrification in lakes (Brzozowska and Gawrońska 2009). Consistently, the oxygenated hypolimnion of Lake Baldegg displayed peak nitrification rates of 87 nM d^{-1}, significantly

19395590, 2026, 1, Downloaded from https://aslopubs.onlinelibrary.wiley.com/doi/10.1002/lno.70281 by Moritz F. Lehmann - Universitat Basel , Wiley Online Library on [16/01/2026]. See the Terms and Conditions (https://onlinelibrary.wiley.com/terms-and-conditions) on Wiley Online Library for rules of use; OA articles are governed by the applicable Creative Commons License

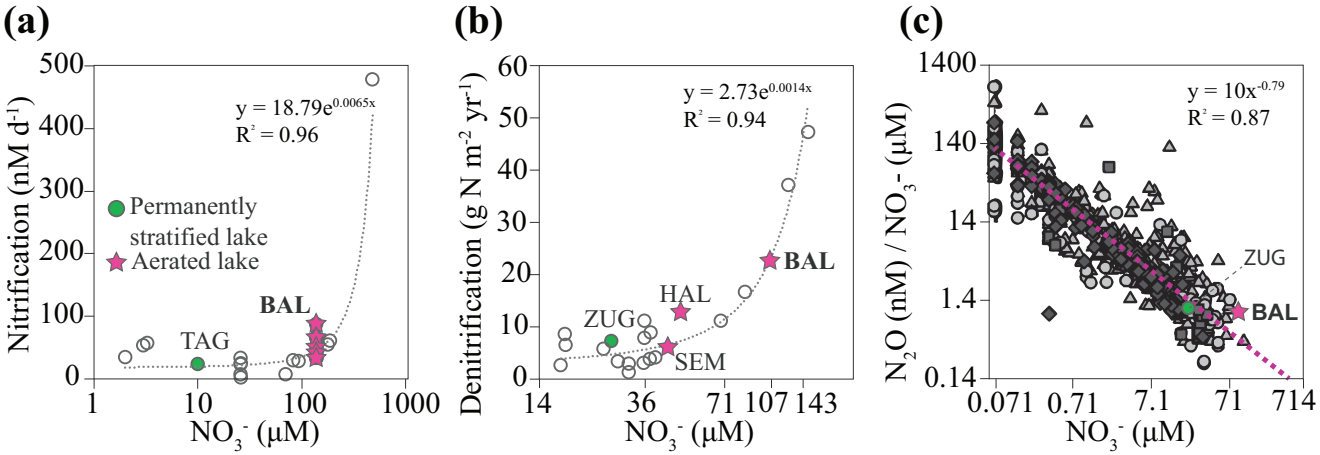

Fig. 7. Effects of aeration/oxygenation in Lake Baldegg on nitrification, denitrification, and N_2O concentrations compared to non-aerated lakes spanning different trophic states. (**a–c**) To facilitate comparisons across lakes of varying trophic states, we analyzed each process in relation to water-column nitrate concentration. Trend lines indicate normalized averages from literature values measured in non-aerated lakes. (a) Relationship between maximum nitrification rates and peak water column nitrate concentrations. Values were compiled from various literature studies on freshwater lakes (white circles; Carini and Joye 2008; Small et al. 2013; Cavaliere and Baulch 2019; Massé et al. 2019; Callbeck et al. 2021; Klotz et al. 2022). Lake Baldegg (BAL), the aerated lake studied here, is shown alongside Lake Tanganyika (TAG), a stratified lake. An exponential curve was fitted to the data, with the slope and R^2 values indicated. (b) Relationship between denitrification rates and water column nitrate concentrations across 21 Swiss lakes (white circles). Lake Baldegg (BAL) is highlighted, along with other aerated lakes in Switzerland (Lake Hallwil, HAL; Lake Sempach, SEM). Lake Zug (ZUG), a meromictic lake, is also shown. Data were originally presented by Müller et al. (2022) and are reproduced under a Creative Commons Attribution 4.0 license: https://creativecommons.org/licenses/by/4.0/. The figure was modified to include an exponential fit, with slope and R^2 values shown. (c) Relationship between N_2O concentrations and NO_3^- concentrations across lakes of varying trophic states in a boreal landscape: nutrient-rich and calcareous (circles), humic small (triangles), humic large (squares), and clear water lakes (diamonds) collected by Kortelainen et al. (2020). Data from Kortelainen et al. (2020) are reproduced under a Creative Commons Attribution 4.0 license: https://creativecommons.org/licenses/by/4.0/. A power regression (purple line) was applied, with the equation provided by Kortelainen et al. (2020). Lakes Baldegg and Zug fall within ± 3 standard deviations of the data and are therefore not statistical outliers, but do deviate from the relationship in Finnish lakes.

higher than those in non-aerated lakes (Fig. 7a) (Carini and Joye 2008; Small et al. 2013; Cavaliere and Baulch 2019; Massé et al. 2019; Callbeck et al. 2021; Klotz et al. 2022; Müller et al. 2022). Artificial aeration likely intensifies the nitrification–denitrification coupling (Brzozowska and Gawrońska 2009), thus, Lake Baldegg should display a greater fixed-N removal capacity than non-aerated systems. However, when normalized for the trophic state, its N-removal efficiency is comparable to that of non-aerated Swiss lakes (Fig. 7b). This pattern is also valid for other artificially aerated Swiss lakes. Although aeration is not primarily intended for N removal, studies have highlighted its role in facilitating fixed-N removal, making our observations unexpected. A possible explanation is that elevated O_2 may stimulate DNRA over denitrification (Cojean et al. 2019), enhancing fixed-N retention through nitrification-DNRA coupling. Although natural-abundance NO_3^- stable isotope measurements cannot distinguish between DNRA and denitrification, their coexistence in the sediments suggests that NH_4^+ can be cycled both through nitrification-DNRA and/or nitrification–denitrification pathways (Baumann et al. 2022, 2024). While oxygenation in Lake Baldegg accelerates nitrification, it does not seem to enhance fixed-N removal via denitrification.

However, the elevated nitrification activity in Lake Baldegg appears to produce high N_2O concentrations and atmospheric N_2O fluxes. Mengis et al. (1997) reported higher N_2O concentrations and emissions in aerated systems (e.g., Lakes Baldegg and Sempach) than in non-aerated lakes. A broader comparative lake survey confirms that N_2O concentrations in Lake Baldegg exceed those of most other lakes (Fig. 7c; Kortelainen et al. 2020), likely due to its high nitrification potential (Fig. 7a). These findings raise concerns about the unintended consequences of artificial aeration, particularly enhanced N_2O emissions. By comparison, the naturally, permanently stratified Lake Zug, serving as a "Baldegg-analogue" under non-aerated conditions, shows baseline N_2O concentrations and denitrification capacity (Fig. 7b,c). Moreover, the lake's anoxic water column favors OM preservation and greater N burial compared to Lake Baldegg (Fiskal et al. 2019; Müller et al. 2022), supporting long-term N removal. Altogether, these findings suggest that artificial aeration does not clearly promote N removal but may instead enhance N_2O emissions, highlighting potential trade-offs in lake management.

Conclusion

This study emphasizes the central role of nitrification in modulating internal N recycling and greenhouse gas dynamics in Lake Baldegg, particularly through its influence on enhanced NO_3^- and N_2O production driven by artificial

19395590, 2026, 1, Downloaded from https://aslopubs.onlinelibrary.wiley.com/doi/10.1002/lno.70281 by Moritz F. Lehmann - Universitat Basel , Wiley Online Library on [16/01/2026]. See the Terms and Conditions (https://onlinelibrary.wiley.com/terms-and-conditions) on Wiley Online Library for rules of use; OA articles are governed by the applicable Creative Commons License

oxygenation and aeration. We demonstrate that nitrification sustained over 80% of the total NO_3^- consumption in the hypolimnion during stratification, contrasting with its rather limited role in the epilimnion (5.3%), where external N inputs exert a more substantial influence.

Our findings reveal a dual-edged impact of artificial oxygenation, and consequently enhanced nitrification. Firstly, it supports and enhances NO_3^- consumption processes (e.g., assimilation and DNRA/denitrification), with the potential to increase the lake's capacity for fixed-N removal. However, this anticipated benefit appears limited in practice, as Lake Baldegg's denitrification efficiency does not significantly exceed that of non-aerated lakes. Secondly, artificial oxygenation also drives elevated N_2O production and emissions, with transport and atmospheric release especially during winter overturn. These outcomes highlight the need for carefully balanced management strategies to optimize nutrient removal while minimizing environmental trade-offs.

This study also demonstrates the value of integrating natural-abundance N and O stable isotope analyses with process rate measurements (i.e., NH_4^+ oxidation), to quantify internal N recycling pathways that would otherwise go untraced by concentration measurements alone. Although the N isotope mass-balance model proved effective, the study could benefit from additional data, such as atmospheric N deposition and N_2 fixation rates, to better constrain the overall N budget and refine estimates of individual N pool sizes. Such data would also clarify the contribution of specific N fluxes to the observed dual NO_3^- isotopic signatures, thereby improving our understanding of apparent NO_3^- isotope anomalies in the lacustrine NO_3^- pool.

Author Contributions

Conceptualization: Alessandra Mazzoli, Claudia Frey, and Moritz F. Lehmann. Data curation: Alessandra Mazzoli. Formal analysis and investigation: Alessandra Mazzoli, Claudia Frey, Cameron M. Callbeck, and Chiara Piantoni. Funding acquisition: Moritz F. Lehmann. Resources: Moritz F. Lehmann. Supervision: Moritz F. Lehmann. Visualization: Alessandra Mazzoli and Cameron M. Callbeck. Writing – original draft preparation: Alessandra Mazzoli, Claudia Frey, Cameron M. Callbeck, and Moritz F. Lehmann. Writing – review and editing: All co-authors.

Acknowledgments

We thank Carsten Schubert's lab for the access to field and lab resources. We acknowledge Karin Beck, Patrick Kathriner, Thomas Kuhn, Judith Kobler, and all student assistants for technical assistance in the field and the laboratory. We would also like to thank Tuula Larmola for her assistance in analyzing the correlative trends in the boreal landscape data. To correct grammatical errors and improve readability, ChatGPT was employed. This study was funded by the Swiss National Science Foundation, grant SNF 188728. Open access publishing facilitated by Universitat Basel, as part of the Wiley - Universitat Basel agreement via the Consortium Of Swiss Academic Libraries.

Conflicts of Interest

None declared.

Data Availability Statement

All field data and isotope mass-balance model outcomes are available on Zenodo (https://doi.org/10.5281/zenodo.15229683).

References

Baumann, K. B. L., A. Mazzoli, G. Salazar, et al. 2024. "Metagenomic and -Transcriptomic Analyses of Microbial Nitrogen Transformation Potential, and Gene Expression in Swiss Lake Sediments." *ISME Communications* 4: ycae110. https://doi.org/10.1093/ismeco/ycae110.

Baumann, K. B. L., R. Thoma, C. M. Callbeck, et al. 2022. "Microbial Nitrogen Transformation Potential in Sediments of Two Contrasting Lakes Is Spatially Structured But Seasonally Stable." *M Sphere* 7: e01013-21. https://doi.org/10.1128/msphere.01013-21.

Botrel, M., L. A. Bristow, M. A. Altabet, I. Gregory-Eaves, and R. Maranger. 2017. "Assimilation and Nitrification in Pelagic Waters: Insights Using Dual Nitrate Stable Isotopes ($\delta^{15}N$, $\delta^{18}O$) in a Shallow Lake." *Biogeochemistry* 135: 221–237. https://doi.org/10.1007/s10533-017-0369-y.

Bourbonnais, A., M. F. Lehmann, J. J. Waniek, and D. E. Schulz-Bull. 2009. "Nitrate Isotope Anomalies Reflect N_2 Fixation in the Azores Front Region (Subtropical NE Atlantic)." *Journal of Geophysical Research: Oceans* 114: C03003. https://doi.org/10.1029/2007JC004617.

Brzozowska, R., and H. Gawrońska. 2009. "The Influence of a Long-Term Artificial Aeration on the Nitrogen Compounds Exchange Between Bottom Sediments and Water in Lake Długie." *Oceanological and Hydrobiological Studies* 38: 113–119. https://doi.org/10.2478/v10009-009-0010-z.

Buergi, H. R., and R. Stadelmann. 2000. "Change of Phytoplankton Diversity during Long-Term Restoration of Lake Baldegg (Switzerland)." *SIL Proceedings, 1922–2010* 27: 574–581. https://doi.org/10.1080/03680770.1998.11901300.

Callbeck, C. M., B. Ehrenfels, K. B. L. Baumann, B. Wehrli, and C. J. Schubert. 2021. "Anoxic Chlorophyll Maximum Enhances Local Organic Matter Remineralization and Nitrogen Loss in Lake Tanganyika." *Nature Communications* 12: 830. https://doi.org/10.1038/s41467-021-21115-5.

Carini, S. A., and S. B. Joye. 2008. "Nitrification in Mono Lake, California: Activity and Community Composition During Contrasting Hydrological Regimes." *Limnology and Oceanography* 53: 2546–2557. https://doi.org/10.4319/lo.2008.53.6.2546.

19395590, 2026, 1, Downloaded from https://aslopubs.onlinelibrary.wiley.com/doi/10.1002/lno.70281 by Moritz F. Lehmann - Universitat Basel , Wiley Online Library on [16/01/2026]. See the Terms and Conditions (https://onlinelibrary.wiley.com/terms-and-conditions) on Wiley Online Library for rules of use; OA articles are governed by the applicable Creative Commons License

Casciotti, K. L., D. M. Sigman, M. G. Hastings, J. K. Böhlke, and A. Hilkert. 2002. "Measurement of the Oxygen Isotopic Composition of Nitrate in Seawater and Freshwater Using the Denitrifier Method." *Analytical Chemistry* 74: 4905–4912. https://doi.org/10.1021/ac020113w.

Casciotti, K. L., T. W. Trull, D. M. Glover, and D. Davies. 2008. "Constraints on Nitrogen Cycling at the Subtropical North Pacific Station ALOHA From Isotopic Measurements of Nitrate and Particulate Nitrogen." *Deep Sea Research Part II: Topical Studies in Oceanography* 55: 1661–1672. https://doi.org/10.1016/j.dsr2.2008.04.017.

Cavaliere, E., and H. M. Baulch. 2019. "Winter Nitrification in Ice-Covered Lakes." *PLoS One* 14: e0224864. https://doi.org/10.1371/journal.pone.0224864.

Cojean, A. N. Y., J. Zopfi, A. Gerster, C. Frey, F. Lepori, and M. F. Lehmann. 2019. "Direct O_2 Control on the Partitioning Between Denitrification and Dissimilatory Nitrate Reduction to Ammonium in Lake Sediments." *Biogeosciences* 16: 4705–4718. https://doi.org/10.5194/bg-16-4705-2019.

Cottingham, P. D., T. H. Davies, and B. T. Hart. 1999. "Aeration to Promote Nitrification in Constructed Wetlands." *Environmental Technology* 20: 69–75. https://doi.org/10.1080/09593332008616794.

Dale, A. W., D. Clemens, K. Dähnke, et al. 2022. "Nitrogen Cycling in Sediments on the NW African Margin Inferred From N and O Isotopes in Benthic Chambers." *Frontiers in Marine Science* 9. https://doi.org/10.3389/fmars.2022.902062.

Finlay, J. C., G. E. Small, and R. W. Sterner. 2013. "Human Influences on Nitrogen Removal in Lakes." *Science* 342: 247–250. https://doi.org/10.1126/science.1242575.

Fiskal, A., L. Deng, A. Michel, et al. 2019. "Effects of Eutrophication on Sedimentary Organic Carbon Cycling in Five Temperate Lakes." *Biogeosciences* 16: 3725–3746. https://doi.org/10.5194/bg-16-3725-2019.

Frame, C. H., and K. L. Casciotti. 2010. "Biogeochemical Controls and Isotopic Signatures of Nitrous Oxide Production by a Marine Ammonia-Oxidizing Bacterium." *Biogeosciences* 7: 2695–2709. https://doi.org/10.5194/bg-7-2695-2010.

Frey, C., J. W. Dippner, and M. Voss. 2014. "Close Coupling of N-Cycling Processes Expressed in Stable Isotope Data at the Redoxcline of the Baltic Sea." *Global Biogeochemical Cycles* 28: 974–991. https://doi.org/10.1002/2013GB004642.

Fuchsman, C. A., B. Paul, J. T. Staley, E. V. Yakushev, and J. W. Murray. 2019. "Detection of Transient Denitrification During a High Organic Matter Event in the Black Sea." *Global Biogeochemical Cycles* 33: 143–162. https://doi.org/10.1029/2018GB006032.

Gächter, R., and B. Wehrli. 1998. "Ten Years of Artificial Mixing and Oxygenation: No Effect on the Internal Phosphorus Loading of Two Eutrophic Lakes." *Environmental Science & Technology* 32: 3659–3665. https://doi.org/10.1021/es980418l.

Gaye, B., B. Nagel, K. Dähnke, T. Rixen, and K. C. Emeis. 2013. "Evidence of Parallel Denitrification and Nitrite Oxidation in the ODZ of the Arabian Sea From Paired Stable Isotopes of Nitrate and Nitrite." *Global Biogeochemical Cycles* 27: 1059–1071. https://doi.org/10.1002/2011GB004115.

Granger, J., D. M. Sigman, J. A. Needoba, and P. J. Harrison. 2004. "Coupled Nitrogen and Oxygen Isotope Fractionation of Nitrate During Assimilation by Cultures of Marine Phytoplankton." *Limnology and Oceanography* 49: 1763–1773. https://doi.org/10.4319/lo.2004.49.5.1763.

Gruber, N., and J. N. Galloway. 2008. "An Earth-System Perspective of the Global Nitrogen Cycle." *Nature* 451: 293–296. https://doi.org/10.1038/nature06592.

Han, H., X. Lu, F. B. David, U. M. Joshi, and L. Zhang. 2014. "Nitrogen Dynamics at the Sediment-Water Interface in a Tropical Reservoir." *Ecological Engineering* 73: 146–153. https://doi.org/10.1016/j.ecoleng.2014.09.016.

Harrison, J. A., R. J. Maranger, R. B. Alexander, et al. 2009. "The Regional and Global Significance of Nitrogen Removal in Lakes and Reservoirs." *Biogeochemistry* 93: 143–157. https://doi.org/10.1007/s10533-008-9272-x.

Higgins, S. N., M. J. Paterson, R. E. Hecky, D. W. Schindler, J. J. Venkiteswaran, and D. L. Findlay. 2018. "Biological Nitrogen Fixation Prevents the Response of a Eutrophic Lake to Reduced Loading of Nitrogen: Evidence From a 46-Year Whole-Lake Experiment." *Ecosystems* 21: 1088–1100. https://doi.org/10.1007/s10021-017-0204-2.

Holtappels, M., G. Lavik, M. M. Jensen, and M. M. M. Kuypers. 2011. "^{15}N-Labeling Experiments to Dissect the Contributions of Heterotrophic Denitrification and Anammox to Nitrogen Removal in the OMZ Waters of the Ocean." In Methods in Enzymology, 223–251. Elsevier. https://doi.org/10.1016/B978-0-12-381294-0.00010-9.

Huttunen, J. T., T. Hammar, J. Alm, J. Silvola, and P. J. Martikainen. 2001. "Greenhouse Gases in Non-Oxygenated and Artificially Oxygenated Eutrophied Lakes During Winter Stratification." *Journal of Environmental Quality* 30: 387–394. https://doi.org/10.2134/jeq2001.302387x.

Jensen, M. M., P. Lam, N. P. Revsbech, et al. 2011. "Intensive Nitrogen Loss Over the Omani Shelf Due to Anammox Coupled With Dissimilatory Nitrite Reduction to Ammonium." *ISME Journal* 5: 1660–1670. https://doi.org/10.1038/ismej.2011.44.

Ji, Q., E. Buitenhuis, P. Suntharalingam, J. L. Sarmiento, and B. B. Ward. 2018. "Global Nitrous Oxide Production Determined by Oxygen Sensitivity of Nitrification and Denitrification." *Global Biogeochemical Cycles* 32: 1790–1802. https://doi.org/10.1029/2018GB005887.

Kelly, C. L., N. M. Travis, P. A. Baya, and K. L. Casciotti. 2021. "Quantifying Nitrous Oxide Cycling Regimes in the Eastern Tropical North Pacific Ocean With Isotopomer Analysis." *Global Biogeochemical Cycles* 35. https://doi.org/10.1029/2020GB006637.

Kelly, C. L., N. M. Travis, P. A. Baya, et al. 2024. "Isotopomer Labeling and Oxygen Dependence of Hybrid Nitrous Oxide

19395590, 2026, 1, Downloaded from https://aslopubs.onlinelibrary.wiley.com/doi/10.1002/lno.70281 by Moritz F. Lehmann - Universitat Basel , Wiley Online Library on [16/01/2026]. See the Terms and Conditions (https://onlinelibrary.wiley.com/terms-and-conditions) on Wiley Online Library for rules of use; OA articles are governed by the applicable Creative Commons License

Production." *Biogeosciences* 21: 3215–3238. https://doi.org/10.5194/egusphere-2023-2642.

Kendall, C., E. M. Elliott, and S. D. Wankel. 2007. "Tracing Anthropogenic Inputs of Nitrogen to Ecosystems." In Stable Isotopes in Ecology and Environmental Science, edited by R. Michener and K. Lajtha, 375–449. Blackwell Pub.

Klotz, F., K. Kitzinger, D. K. Ngugi, et al. 2022. "Quantification of Archaea-Driven Freshwater Nitrification From Single Cell to Ecosystem Levels." *The ISME Journal* 16: 1647–1656. https://doi.org/10.1038/s41396-022-01216-9.

Kortelainen, P., T. Larmola, M. Rantakari, S. Juutinen, J. Alm, and P. J. Martikainen. 2020. "Lakes as Nitrous Oxide Sources in the Boreal Landscape." *Global Change Biology* 26: 1432–1445. https://doi.org/10.1111/gcb.14928.

Lehmann, M. F., S. M. Bernasconi, A. Barbieri, M. R. Simona, and J. A. McKenzie. 2004*a*. "Interannual Variation of the Isotopic Composition of Sedimenting Organic Carbon and Nitrogen in Lake Lugano: A Long-Term Sediment Trap Study." *Limnology and Oceanography* 49: 839–849. https://doi.org/10.4319/lo.2004.49.3.0839.

Lehmann, M. F., S. M. Bernasconi, J. A. Mckenzie, A. Barbieri, M. Simona, and M. Veronesi. 2004*b*. "Seasonal Variation of the $\delta^{13}C$ and $\delta^{15}N$ of Particulate and Dissolved Carbon and Nitrogen in Lake Lugano: Constraints on Biogeochemical Cycling in a Eutrophic Lake." *Limnology and Oceanography* 49: 415–429. https://doi.org/10.4319/lo.2004.49.2.0415.

Lehmann, M. F., D. M. Sigman, and W. M. Berelson. 2004*c*. "Coupling the $^{15}N/^{14}N$ and $^{18}O/^{16}O$ of Nitrate as a Constraint on Benthic Nitrogen Cycling." *Marine Chemistry* 88: 1–20. https://doi.org/10.1016/j.marchem.2004.02.001.

Lehmann, M. F., D. M. Sigman, D. C. McCorkle, et al. 2007. "The Distribution of Nitrate $^{15}N/^{14}N$ in Marine Sediments and the Impact of Benthic Nitrogen Loss on the Isotopic Composition of Oceanic Nitrate." *Geochimica et Cosmochimica Acta* 71: 5384–5404. https://doi.org/10.1016/j.gca.2007.07.025.

Li, F., L. Lu, X. Zheng, et al. 2014. "Enhanced Nitrogen Removal in Constructed Wetlands: Effects of Dissolved Oxygen and Step-Feeding." *Bioresource Technology* 169: 395–402. https://doi.org/10.1016/j.biortech.2014.07.004.

Li, S., A. Yue, S. S. Moore, et al. 2022. "Temperature-Related N_2O Emission and Emission Potential of Freshwater Sediment." *PRO* 10: 2728. https://doi.org/10.3390/pr10122728.

Li, Y., H. Tian, Y. Yao, et al. 2024. "Increased Nitrous Oxide Emissions From Global Lakes and Reservoirs Since the Pre-Industrial Era." *Nature Communications* 15: 942. https://doi.org/10.1038/s41467-024-45061-0.

Liang, X., B. Wang, D. Gao, et al. 2022. "Nitrification Regulates the Spatiotemporal Variability of N_2O Emissions in a Eutrophic Lake." *Environmental Science & Technology* 56: 17430–17442. https://doi.org/10.1021/acs.est.2c03992.

Liboriussen, L., M. Søndergaard, E. Jeppesen, et al. 2009. "Effects of Hypolimnetic Oxygenation on Water Quality: Results From Five Danish Lakes." *Hydrobiologia* 625: 157–172. https://doi.org/10.1007/s10750-009-9705-0.

Liu, D., J. Zhong, X. Zheng, C. Fan, J. Yu, and W. Zhong. 2018. "N_2O Fluxes and Rates of Nitrification and Denitrification at the Sediment–Water Interface in Taihu Lake, China." *Water* 10: 911. https://doi.org/10.3390/w10070911.

Massé, S., M. Botrel, D. A. Walsh, and R. Maranger. 2019. "Annual Nitrification Dynamics in a Seasonally Ice-Covered Lake." *PLoS One* 14: e0213748. https://doi.org/10.1371/journal.pone.0213748.

McCarthy, M. J., W. S. Gardner, M. F. Lehmann, A. Guindon, and D. F. Bird. 2016. "Benthic Nitrogen Regeneration, Fixation, and Denitrification in a Temperate, Eutrophic Lake: Effects on the Nitrogen Budget and Cyanobacteria Blooms." *Limnology and Oceanography* 61: 1406–1423. https://doi.org/10.1002/lno.10306.

McIlvin, M. R., and K. L. Casciotti. 2010. "Fully Automated System for Stable Isotopic Analyses of Dissolved Nitrous Oxide at Natural Abundance Levels." *Limnology and Oceanography: Methods* 8: 54–66. https://doi.org/10.4319/lom.2010.8.54.

Mengis, M., R. Gächter, and B. Wehrli. 1997. "Sources and Sinks of Nitrous Oxide (N_2O) in Deep Lakes." *Biogeochemistry* 38: 281–301. https://doi.org/10.1023/A:1005814020322.

Mostefa, G., and K. Ahmed. 2012. "Treatment of Water Supplies by the Technique of Dynamic Aeration." *Procedia Engineering* 33: 209–214. https://doi.org/10.1016/j.proeng.2012.01.1195.

Müller, B., J. S. Meyer, and R. Gächter. 2022. "Denitrification and Nitrogen Burial in Swiss Lakes." *Environmental Science & Technology* 56: 2794–2802. https://doi.org/10.1021/acs.est.1c07602.

Müller, B., R. Thoma, K. B. L. Baumann, C. M. Callbeck, and C. J. Schubert. 2021. "Nitrogen Removal Processes in Lakes of Different Trophic States From On-Site Measurements and Historic Data." *Aquatic Sciences* 83: 37. https://doi.org/10.1007/s00027-021-00795-7.

Pai, S.-C., C.-C. Yang, and J. P. Riley. 1990. "Formation Kinetics of the Pink Azo Dye in the Determination of Nitrite in Natural Waters." *Analytica Chimica Acta* 232: 345–349. https://doi.org/10.1016/S0003-2670(00)81252-0.

Robertson, E. K., K. L. Roberts, L. D. W. Burdorf, P. Cook, and B. Thamdrup. 2016. "Dissimilatory Nitrate Reduction to Ammonium Coupled to Fe(II) Oxidation in Sediments of a Periodically Hypoxic Estuary." *Limnology and Oceanography* 61: 365–381. https://doi.org/10.1002/lno.10220.

Scott, J. T., M. J. McCarthy, and H. W. Paerl. 2019. "Nitrogen Transformations Differentially Affect Nutrient-Limited Primary Production in Lakes of Varying Trophic State." *Limnology and Oceanography Letters* 4: 96–104. https://doi.org/10.1002/lol2.10109.

Seitzinger, S., J. A. Harrison, J. K. Böhlke, et al. 2006. "Denitrification Across Landscapes and Waterscapes: A Synthesis." *Ecological Applications* 16: 2064–2090. https://doi.org/10.1890/1051-0761(2006)016[2064:DALAWA]2.0.CO;2.

19395590, 2026, 1, Downloaded from https://aslopubs.onlinelibrary.wiley.com/doi/10.1002/lno.70281 by Moritz F. Lehmann - Universitat Basel , Wiley Online Library on [16/01/2026]. See the Terms and Conditions (https://onlinelibrary.wiley.com/terms-and-conditions) on Wiley Online Library for rules of use; OA articles are governed by the applicable Creative Commons License

Sigman, D. M., K. L. Casciotti, M. Andreani, C. Barford, M. Galanter, and J. K. Böhlke. 2001. "A Bacterial Method for the Nitrogen Isotopic Analysis of Nitrate in Seawater and Freshwater." *Analytical Chemistry* 73: 4145–4153. https://doi.org/10.1021/ac010088e.

Sigman, D. M., and F. Fripiat. 2019. "Nitrogen Isotopes in the Ocean." In Encyclopedia of Ocean Sciences, vol. 1–5, 3rd ed., 263–278. Elsevier.

Sigman, D. M., J. Granger, P. J. DiFiore, et al. 2005. "Coupled Nitrogen and Oxygen Isotope Measurements of Nitrate along the Eastern North Pacific Margin." *Global Biogeochemical Cycles* 19: GB4022. https://doi.org/10.1029/2005GB002458.

Singleton, V. L., and J. C. Little. 2006. "Designing Hypolimnetic Aeration and Oxygenation Systems—A Review." *Environmental Science & Technology* 40: 7512–7520. https://doi.org/10.1021/es060069s.

Small, G. E., G. S. Bullerjahn, R. W. Sterner, et al. 2013. "Rates and Controls of Nitrification in a Large Oligotrophic Lake." *Limnology and Oceanography* 58: 276–286. https://doi.org/10.4319/lo.2013.58.1.0276.

Stein, L. Y., and M. G. Klotz. 2016. "The Nitrogen Cycle." *Current Biology* 26: 94–98. https://doi.org/10.1016/j.cub.2015.12.021.

Tadonleke, R. D., J. Lazzarotto, O. Anneville, and J.-C. Druart. 2009. "Phytoplankton Productivity Increased in Lake Geneva Despite Phosphorus Loading Reduction." *Journal of Plankton Research* 31: 1179–1194. https://doi.org/10.1093/plankt/fbp063.

Thamdrup, B., and T. Dalsgaard. 2002. "Production of N_2 Through Anaerobic Ammonium Oxidation Coupled to Nitrate Reduction in Marine Sediments." *Applied and Environmental Microbiology* 68: 1312–1318. https://doi.org/10.1128/AEM.68.3.1312-1318.2002.

Wankel, S. D., C. Kendall, J. T. Pennington, F. P. Chavez, and A. Paytan. 2007. "Nitrification in the Euphotic Zone as Evidenced by Nitrate Dual Isotopic Composition: Observations From Monterey Bay, California." *Global Biogeochemical Cycles* 21: GB2009. https://doi.org/10.1029/2006GB002723.

Wenk, C. B., C. H. Frame, K. Koba, et al. 2016. "Differential N_2O Dynamics in Two Oxygen-Deficient Lake Basins Revealed by Stable Isotope and Isotopomer Distributions." *Limnology and Oceanography* 61: 1735–1749. https://doi.org/10.1002/lno.10329.

Wenk, C. B., J. Zopfi, J. Blees, M. Veronesi, H. Niemann, and M. F. Lehmann. 2014. "Community N and O Isotope Fractionation by Sulfide-Dependent Denitrification and Anammox in a Stratified Lacustrine Water Column." *Geochimica et Cosmochimica Acta* 125: 551–563. https://doi.org/10.1016/j.gca.2013.10.034.

Xia, X., T. Liu, Z. Yang, et al. 2017. "Enhanced Nitrogen Loss From Rivers Through Coupled Nitrification-Denitrification Caused by Suspended Sediment." *Science of the Total Environment* 579: 47–59. https://doi.org/10.1016/j.scitotenv.2016.10.181.

Xu, S., P. Kang, and Y. Sun. 2016. "A Stable Isotope Approach and Its Application for Identifying Nitrate Source and Transformation Process in Water." *Environmental Science and Pollution Research* 23: 1133–1148. https://doi.org/10.1007/s11356-015-5309-6.

Yang, J. Y. T., J. M. Tang, S. Kang, et al. 2022. "Comparison of Nitrate Isotopes Between the South China Sea and Western North Pacific Ocean: Insights Into Biogeochemical Signals and Water Exchange." *Journal of Geophysical Research: Oceans* 127: e2021JC018304. https://doi.org/10.1029/2021JC018304.

Yeerken, S., L. Li, M. Deng, K. Song, and F. Wu. 2023. "Effect and Microbial Mechanism of Suspended Sediments Particle Size on Nitrous Oxide Emission in Eutrophic Lakes." *Environmental Pollution* 334: 122180. https://doi.org/10.1016/j.envpol.2023.122180.

Yu, L., E. Harris, D. Lewicka-Szczebak, et al. 2020. "What Can we Learn From N_2O Isotope Data?—Analytics, Processes and Modelling." *Rapid Communications in Mass Spectrometry* 34: e8858. https://doi.org/10.1002/rcm.8858.

Zhou, Y., X. Xu, R. Han, et al. 2019. "Suspended Particles Potentially Enhance Nitrous Oxide (N_2O) Emissions in the Oxic Estuarine Waters of Eutrophic Lakes: Field and Experimental Evidence." *Environmental Pollution* 252: 1225–1234. https://doi.org/10.1016/j.envpol.2019.06.076.

Supporting Information

Additional Supporting Information may be found in the online version of this article.

Submitted 12 May 2025
Revised 01 November 2025
Accepted 13 November 2025

19395590, 2026, 1, Downloaded from https://aslopubs.onlinelibrary.wiley.com/doi/10.1002/lno.70281 by Moritz F. Lehmann - Universitat Basel , Wiley Online Library on [16/01/2026]. See the Terms and Conditions (https://onlinelibrary.wiley.com/terms-and-conditions) on Wiley Online Library for rules of use; OA articles are governed by the applicable Creative Commons License